Published February 2, 2015

Perlecan is recruited by dystroglycan to nodes of Ranvier and binds the clustering molecule gliomedin

Cristina Colombelli,[1]* Marilena Palmisano,[1,2,3]* Yael Eshed-Eisenbach,[4] Desirée Zambroni,[1] Ernesto Pavoni,[1] Cinzia Ferri,[1] Stefania Saccucci,[1] Sophie Nicole,[5,6,7,8] Raija Soininen,[9] Karen K. McKee,[10] Peter D. Yurchenco,[10] Elior Peles,[4] Lawrence Wrabetz,[1,2,3] and M. Laura Feltri[1,2,3]

[1]Division of Genetics and Cell Biology, San Raffaele Hospital, 20132 Milan, Italy
[2]Department of Biochemistry and [3]Department of Neurology, Hunter James Kelly Research Institute, School of Medicine and Biomedical Sciences, University at Buffalo, Buffalo, NY 14203
[4]Department of Molecular Cell Biology, The Weizmann Institute of Science, Rehovot 76100, Israel
[5]Institut du Cerveau et de la Moelle Épinière, 75013 Paris, France
[6]Institut National de la Santé et de la Recherche Médicale, U1127, 75019 Paris, France
[7]Sorbonne Universités, Université Pierre et Marie Currie, UMRS1127, 75252 Paris, France
[8]Centre National de la Recherche Scientifique, UMR 7225, 75013 Paris, France
[9]Oulu Center for Cell–Extracellular Matrix Research, University of Oulu, 90014 Oulu, Finland
[10]Rutgers University, Piscataway, NJ 08854

Fast neural conduction requires accumulation of Na^+ channels at nodes of Ranvier. Dedicated adhesion molecules on myelinating cells and axons govern node organization. Among those, specific laminins and dystroglycan complexes contribute to Na^+ channel clustering at peripheral nodes by unknown mechanisms. We show that in addition to facing the basal lamina, dystroglycan is found near the nodal matrix around axons, binds matrix components, and participates in initial events of nodogenesis. We identify the dystroglycan-ligand perlecan as a novel nodal component and show that dystroglycan is required for the selective accumulation of perlecan at nodes. Perlecan binds the clustering molecule gliomedin and enhances clustering of node of Ranvier components. These data show that proteoglycans have specific roles in peripheral nodes and indicate that peripheral and central axons use similar strategies but different molecules to form nodes of Ranvier. Further, our data indicate that dystroglycan binds free matrix that is not organized in a basal lamina.

Introduction

Nodes of Ranvier are located at gaps in myelin, where the axolemma is endowed with high densities of voltage-gated Na^+ channels that ensure the regeneration of action potentials during saltatory conduction (Ranvier, 1871; Hodgkin and Huxley, 1952). The way Na^+ channels accumulate at these focal sites is the matter of intense studies. Neurofascin 186 (NF186) is a pioneer molecule that traps Na^+ channels at nodes by linking to glial molecules and to the axonal cytoskeleton (Sherman et al., 2005; Zonta et al., 2008; Thaxton et al., 2011). Additional mechanisms such as barriers formed by adjacent paranodal junctions are required to safeguard node integrity (Feinberg et al., 2010). Peripheral and central nodes have common and distinct features, the most notable being the difference in the overlying glial cell: oligodendrocytes and astrocytic processes in the central nervous system (CNS) versus Schwann cell (SC) microvilli in the peripheral nervous system (PNS; Elfvin, 1961; Peters, 1966; Hildebrand, 1971; Hildebrand and Waxman, 1984; Raine, 1984; Waxman and Black, 1984; Ichimura and Ellisman, 1991).

Both PNS and CNS nodes are embedded in a matrix enriched in nonsulfated mucopolysaccharides, hyaluronic acid, and proteoglycans. Recent work showed that proteoglycans in the CNS constitute a third redundant protection for nodes, such that disruption of more than one mechanism is required to impair Na^+ channel localization and maintenance (Susuki

*C. Colombelli and M. Palmisano contributed equally to this paper.

Correspondence to M.L. Feltri: mlfeltri@buffalo.edu

Abbreviations used in this paper: CNS, central nervous system; DG, Dystroglycan; DRG, dorsal root ganglia; ERM, ezrin/radixin/moesin; HS, heparan sulfate; HSPG, heparan sulfate proteoglycans; IEM, immunoelectron microscopy; NF186, Neurofascin 186; P, postnatal day; PNS, peripheral nervous system; SC, Schwann cell.

Supplemental Material can be found at:
http://jcb.rupress.org/content/suppl/2015/01/30/jcb.201403111.DC1.html
http://jcb.rupress.org/content/suppl/2015/02/02/jcb.201403111.DC2.html

The Rockefeller University Press $30.00
J. Cell Biol. Vol. 208 No. 3 313–329
www.jcb.org/cgi/doi/10.1083/jcb.201403111

Published February 2, 2015

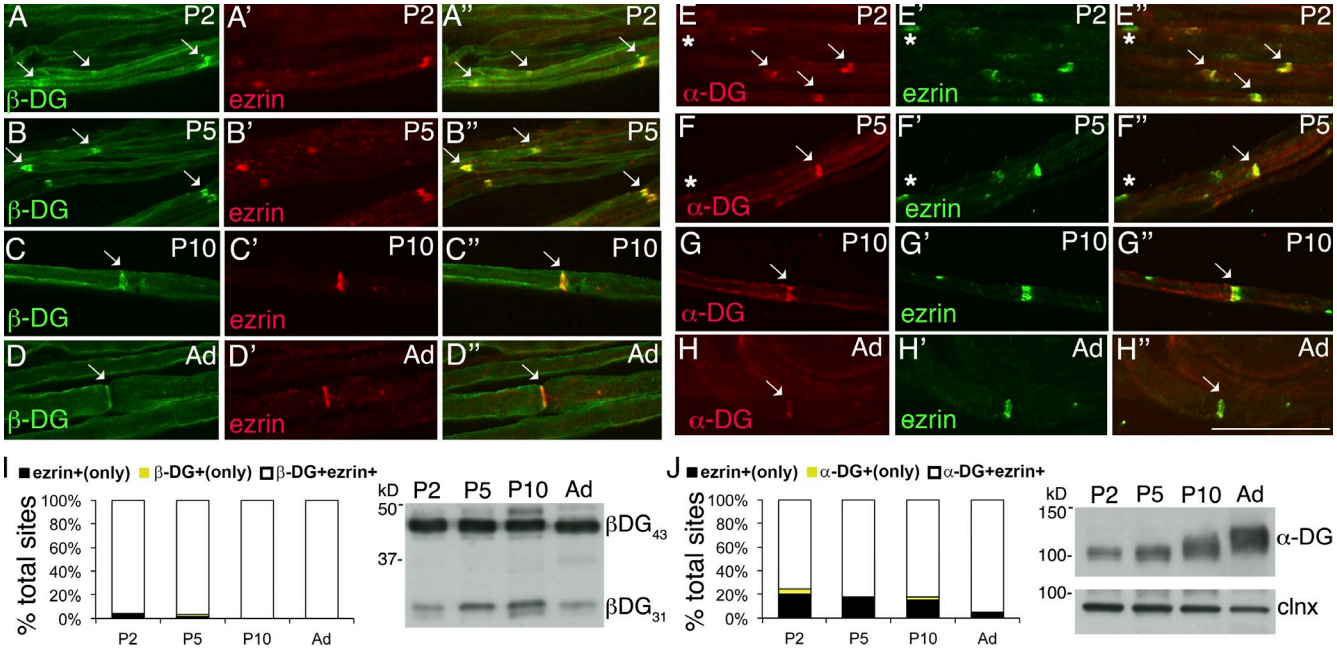

Figure 1. **α- and β-DG are early nodal markers.** Teased fibers from rat sciatic nerves at P2, P5, P10, and adult (Ad). (A–H) Staining for DG (A–D: green β-DG; E–H: red α-DG) and ezrin (A′–H′) and merged confocal images (A″–H″) show that the majority of early nodes stain for DG. Arrows indicate double positive nodes and asterisks indicate DG-negative nodes. Bar, 35 µm. (I and J) Fraction of nodes positive for the indicated markers at different times. Counts are from two or three experiments from six rats per time point; *n* = 69 (P2), 68 (P5), 45 (P10), and 20 (Ad) nodes in I and *n* = 77 (P2), 97 (P5), 24 (P10), and 20 (Ad) nodes in J. Western blot for β-DG (I) or α-DG (J) on developing rat sciatic nerves.

et al., 2013). Whether similar mechanisms exist in peripheral nodes is unknown, but is supported by the observation that gliomedin, a collagen-like molecule that induces clustering of Na^+ channels (Eshed et al., 2005; Feinberg et al., 2010), is incorporated into SC ECM by binding to heparan sulfate proteoglycans (HSPG; Eshed et al., 2007). The PNS nodal gap contains the proteoglycans versican V1 (Apostolski et al., 1994; Melendez-Vasquez et al., 2005), NG2 (Martin et al., 2001), syndecan-3 and -4 (Goutebroze et al., 2003; Melendez-Vasquez et al., 2005), and tenascin (Rieger et al., 1986). According to the current model, SC-derived gliomedin and NrCAM interact with NF186 on the axonal membrane to promote its relocation from internodal regions and its trapping at nascent intermediates called heminodes (Tao-Cheng and Rosenbluth, 1983; Lambert et al., 1997; Schafer et al., 2006; Feinberg et al., 2010; Zhang et al., 2012). Subsequently, NF186 recruits ankyrin-G, αII and βIV spectrin, Na^+ channels, and KCNQ (Lambert et al., 1997; Koticha et al., 2006; Pan et al., 2006; Dzhashiashvili et al., 2007; Voas et al., 2007). Deletion of NF186 in mice prevents Na^+ channel clustering (Sherman et al., 2005; Thaxton et al., 2011), whereas deletion of either gliomedin or NrCAM alone impairs Na^+ channel clustering at heminodes, but not at mature nodes (Custer et al., 2003; Feinberg et al., 2010). This supports a model of tripartite redundant function because lack of both gliomedin and the paranodal molecule Caspr, or both NrCAM and Caspr, severely impairs the accumulation of Na^+ channels at mature nodes (Feinberg et al., 2010).

Dystroglycan (DG) is another glial molecule found in microvilli, and SC-specific ablation of the DG gene causes abnormal clustering of Na^+ channels and disorganization of microvilli (Saito et al., 2003). Similar alterations were found in mice lacking SC laminins and in a merosin-deficient muscular dystrophy patient (Occhi et al., 2005). SC DG comprises an α subunit that binds laminins, agrin, and perlecan in basal laminae and a transmembrane β subunit linked to the cytoskeleton through different dystrophin isoforms. DG and the 116-kD dystrophin (Dp116) are in microvilli, whereas laminins 211 and 511 are enriched in the basal lamina over nodes (Occhi et al., 2005). It is unknown whether DG is required for the formation or maintenance of Na^+ channel clusters and by which mechanism. Here we show that DG is recruited to nascent nodes and is required for the formation of normal heminodes and Na^+ channel clusters. By immunoelectron microscopy (IEM), α- and β-DG are localized at SC microvilli facing both the basal lamina and the axon, suggesting that in addition to its known role as a basal lamina receptor, DG could interact with components of the perinodal matrix. Indeed, we find that the DG ligand perlecan is a novel proteoglycan found in PNS nodes, and that perlecan localization at nodes requires DG. Perlecan binds gliomedin and enhances clustering of nodal components by gliomedin. This work identifies perlecan as a HSPG that binds gliomedin and highlights similarities and differences with the assembly of central nodes.

Results

α- and β-DG are early markers of SC microvilli

α-DG, β-DG, and Dp116 are found at nodes of Ranvier, and laminins 211 and 511 are enriched in the basal lamina over microvilli (Occhi et al., 2005). Ablation of DG in SCs results in small and abnormally shaped Na^+ channel clusters at nodes (Saito et al., 2003; Occhi et al., 2005). To explore if this is

Published February 2, 2015

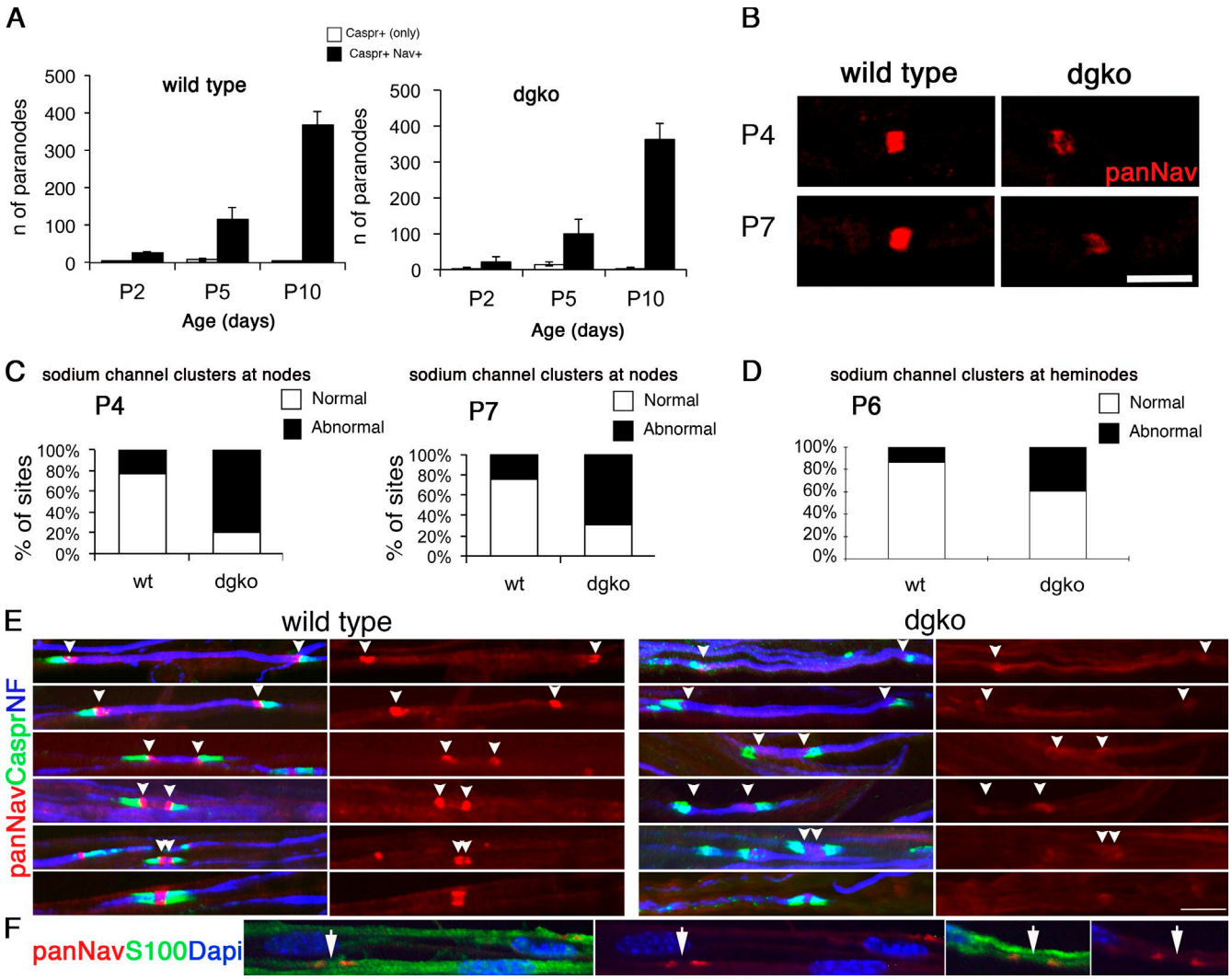

Figure 2. **DG is required for proper Na^+ channel clustering at nascent nodes and heminodes.** (A) Na^+ channel clustering is not delayed in DG-deficient nerves. Number of paranodes (Caspr staining) containing (shaded bars) or devoid (open bars) of Na^+ channels in nerves. Total sites analyzed for wild type were P2, 89; P5, 362; and P10, 1,107; and for dgko, P2, 74; P5, 336; and P10, 786. Results are reported as mean ± SEM of three mice/genotype. (B and C) Na^+ channel clusters form abnormally without DG. Sciatic nerve fibers from P4 and P7 mice stained for pan-Na^+ channels. (B) Mutant clusters are smaller and irregular. (C) More clusters are abnormal in DG mutants (P4, $n = 83$, 79%; P7, $n = 41$, 69.5% in mutant; P4, $n = 27$, 23%; P7, $n = 15$, 23.8% in wild type). $P < 0.001$ mutant versus wild type by χ^2 test; $n = 224$ (P4) and $n = 122$ (P7). (D) Abnormal or absent Na^+ channel clusters at heminodes are more frequent in dgko ($n = 186$; 40%) than control ($n = 49$; 14%). $P < 0.001$ by χ^2 test; $n = 823$ nodes. (E) Teased nerve fibers from P6 nerves labeled for Na^+ channels (red), Caspr (green), and neurofilament (NF; blue). Arrowheads point to the position of developing heminodes/nodes. (F) Staining with S100 (green) shows that SC cytoplasm covers the space between heminodes (arrows). Bars: (B) 4.5 µm; (E and F) 17.5 µm.

caused by defective cluster formation during development or by degeneration of normal clusters over time, we first asked if DG is found in developing nodes by immunostaining sciatic nerve teased fibers. Both α- and β-DG colocalize with ezrin, an early nodal marker, soon after birth (Fig. 1). Western blot analysis confirmed that both glycosylated α-DG, recognized by the glyco-specific antibody IIH6, and the cleaved (β-DG_{31}) and uncleaved form of β-DG (β-DG_{43}) are present at postnatal day 2 (P2; Fig. 1; Yamada et al., 2001; Martin, 2003; Hnia et al., 2006; Zhong et al., 2006; Cai et al., 2007; Court et al., 2011; Walko et al., 2013). In contrast, laminin α5 at P2–P5 is found predominantly in perinuclear regions, and it acquires its nodal localization starting at P10 (Fig. S1). Thus, laminin 511 localizes at nodes after they are formed.

Absence of DG does not interfere with the timing of Na^+ channel cluster formation

We counted the number of clusters flanked by Caspr-positive paranodes at different ages in sciatic nerves of mice deficient in SC-DG and found that at each time point the number of clusters per field of view was similar to wild-type animals (Fig. 2 A). Therefore, the absence of DG does not affect the timing of cluster formation.

Newly formed clusters are already abnormal in the absence of DG

To determine whether DG is required to form or stabilize clusters, we evaluated the morphology of newly formed clusters in mutant nerves at P4 and P7 by immunostaining with anti–pan-Na^+

Published February 2, 2015

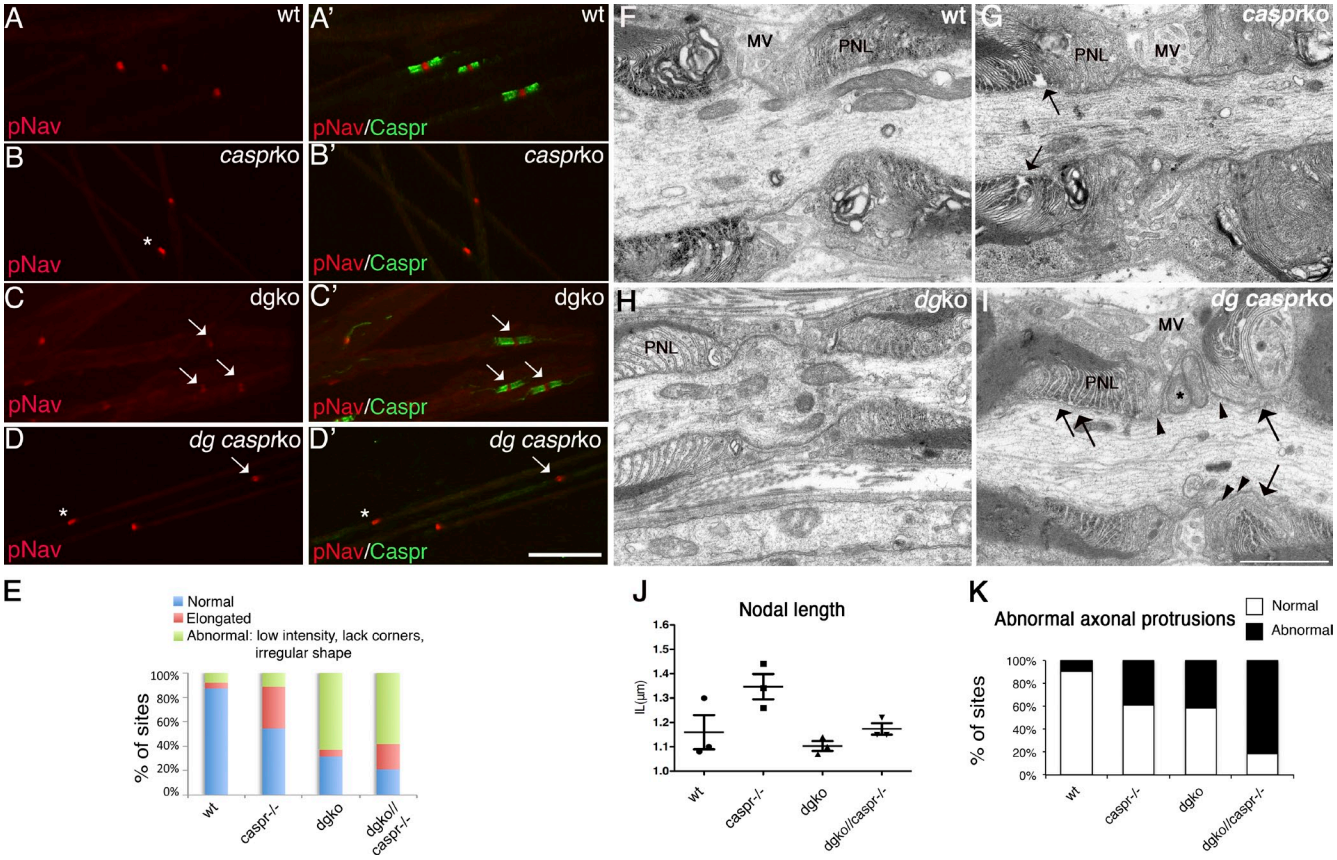

Figure 3. **Nodal abnormalities in DGko/Caspr null mutants.** (A–D) Teased fibers from P28 sciatic nerves. Staining for Na^+ channels (red; A–D) and Caspr (green; A'–D', merged images). Bar, 17.5 µm. (E) Frequency of normal (asterisk) and abnormal (arrow) clusters in P28 mice nerves (79% in dgko//*Caspr*$^{-/-}$, *n* = 102; 69% in dgko, *n* = 72; 45% in *Caspr*$^{-/-}$, *n* = 49; 13% in wild type, *n* = 16). The difference between dgko//*Caspr*$^{-/-}$ and dgko is not statistically significant by Kruskal-Wallis test. (F–I) EM of nodes in P28 sciatic nerves of wild-type (F), single (G and H), and double mutants (I). SC microvilli (MV) and paranodal loops (PNL) are marked. As reported, paranodal loops detach from the axolemma in *Caspr*$^{-/-}$ and dgko//*Caspr*$^{-/-}$ mice (arrows). SC microvilli of dgko//*Caspr*$^{-/-}$ are disorganized and blunt, and occasionally penetrate between the paranodal loops and the axolemma (arrowheads). An elongated axonal protrusion full of mitochondria is shown (I, asterisk). Bar, 1 µm. (J) Mean nodal length in P28 wild-type, *Caspr*$^{-/-}$, dgko, and dgko/*Caspr*$^{-/-}$ sciatic nerves by EM (*n* = 61, 60, 72, and 79, respectively; three mice per genotype). No statistical difference was observed by Student's *t* test. (K) The number of nodal axonal spines at P28 is higher in double mutants (9% in wild type, *n* = 64; 39% in *Caspr*$^{-/-}$, *n* = 70; 41% in dgko, *n* = 80; 82% in dgko//*Caspr*$^{-/-}$, *n* = 82). $P < 0.001$ by χ^2 test.

channel antibodies. Two independent investigators classified clusters blindly as normal (rectangular, with square corners and normal width), or abnormal (irregularly shaped, lacking square corners, diffuse, and long or low intensity in every optical plane; Fig. 2 B) as described previously (Occhi et al., 2005). DG-deficient clusters were frequently abnormal at P4 and P7 (Fig. 2, B and C), as previously described in adult mice (Occhi et al., 2005). Thus, DG is required for proper clustering of nascent Na^+ channels.

Proper clustering of Na^+ channels at heminodes requires DG

In development, Na^+ channels are first redistributed from local axolemma pools to heminodes, through interaction with extracellular molecules (Feinberg et al., 2010; Zhang et al., 2012). Longitudinal growth of the glial processes, which entirely covers the space between heminodes (Fig. 2 F), displaces these heminodal clusters, probably bringing them closer until they fuse and form a single node (Boiko et al., 2001; Pedraza et al., 2001; Eshed-Eisenbach and Peles, 2013). Gliomedin, a component of the nodal matrix that binds NF186 and NrCAM, is required for formation of heminodes (Feinberg et al., 2010). To ask if DG is also involved, we stained developing nerves from wild-type and DG-deficient mice at P6, when both nodes and heminodes can be detected (Schafer et al., 2006; Fig. 2 E). Two independent investigators counted heminodal clusters blindly (identified by the presence of only one flanking Caspr-positive paranode) and classified them as normal or abnormal/absent. The frequency of abnormal or absent clusters was higher in mutants than controls (Fig. 2 D). Thus, DG contributes to the clustering of Na^+ channels at heminodes.

The absence of paranodal junctions slightly worsens the nodal abnormalities of DG-deficient mice

Several overlapping mechanisms ensure Na^+ channel accumulation at nodes. The pioneer molecule NF186 is first redistributed from local pools to heminodes by interacting with NrCAM and gliomedin (Sherman et al., 2005; Feinberg et al., 2010; Thaxton et al., 2011; Zhang et al., 2012). Here NF186 recruits Na^+ channels,

Published February 2, 2015

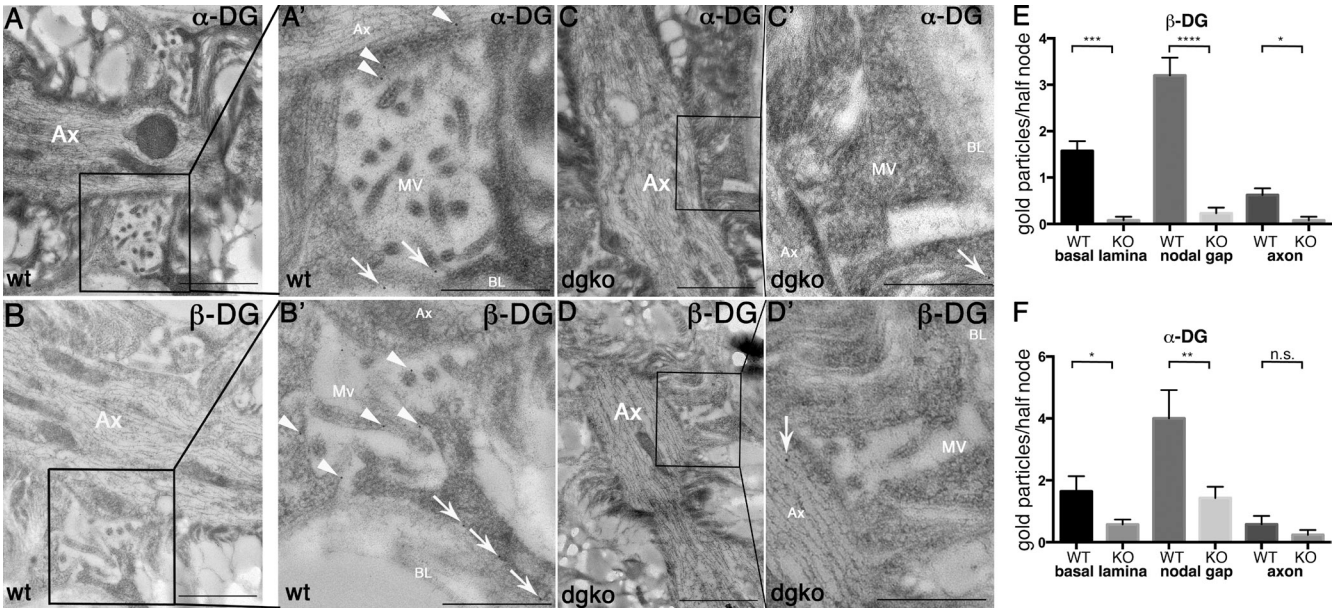

Figure 4. **α- and β-DG localize in the nodal gap.** IEM on sciatic nerve of wild-type (A and B) or dgko (C and D) adult mouse using antibodies against α-DG (A and C) and β-DG (B and D) shows gold particles decorating SC microvilli both near the basal lamina (arrows in A′ and B′, magnified at right), near the axon, and in the nodal gap (arrowheads in A′ and B′, magnified at right) only in wild-type nerves. Occasional gold grains are randomly distributed in the knockout nerves (C′ and D′, arrows). (E and F) Number of gold grains in each half/node. *, P < 0.02; ***, P < 0.0002; ****, P < 0.0001 by Student's *t* test. Error bars represent SEM. Bars: (A–D) 1 µm; (A′–D′) 0.5 µm.

which are then stabilized through ankyrin G and βIV spectrin in the axon (Komada and Soriano, 2002; Lacas-Gervais et al., 2004; Yang et al., 2004; Koticha et al., 2006; Dzhashiashvili et al., 2007) and by formation of paranodes (Feinberg et al., 2010). Disruption of at least two of these mechanisms is necessary to impair Na^+ channel clustering (Feinberg et al., 2010). To ask if disruption of paranodes further impaired nodal clustering in DG mutants, we crossed them with mice lacking the paranodal protein Caspr. Caspr null mice exhibit a progressive neurological defect, but have a normal life span (Bhat et al., 2001; Gollan et al., 2003). Homozygous dgko/*Caspr*$^{-/-}$ mice were similar to *Caspr*$^{-/-}$ mice without worsening of the neurological phenotype. By EM, double mutants showed more severe and frequent nodal defects than single DG mutants. Microvilli were more disorganized, did not attach to the nodal axolemma, and penetrated the space between paranodal loops and axons (Fig. 3, F–I). Axonal protrusions that contained mitochondria and vesicles invaded the nodal gap in place of atrophic microvilli (Fig. 3 I) and were detected with higher frequency (Fig. 3 K). Despite these abnormalities, nodal length was not increased (Fig. 3 J) and nodal clustering of Na^+ channels was not worsened (Fig. 3, A–E).

α- and β-DG localize in the nodal gap

By confocal microscopy, DG colocalizes with ezrin/radixin/moesin (ERM) proteins at SC microvilli (Occhi et al., 2005). To address whether DG is inserted solely in the SC membrane facing the basal lamina, or also in the nodal gap facing the axon, we performed IEM on sciatic nerves. Both α- and β-DG are found in SC microvilli not only adjacent to the basal lamina but also in the nodal gap abutting onto the axon (Fig. 4, A and B). Only occasional gold grains were found in DG-deficient mice (Fig. 4).

In light of the dual localization of α- and β-DG, we hypothesize two different, but not mutually exclusive, mechanisms through which DG aids Na^+ channel clustering. First, by bridging the basal lamina to the cytoskeleton, DG induces cytoskeletal rearrangements required for microvilli to grow radially and internodes to grow longitudinally adjacent to nodes, thus mechanically restricting Na^+ channel. Indeed, DG deficiency in SCs causes microvillar hypotrophy (Saito et al., 2003) and short internodes (Court et al., 2009), and in epithelia DG interacts with ezrin to form cellular protrusions (Spence et al., 2004). The second possibility is that DG also organizes the free ECM in the nodal gap and favors the local presentation of adhesion molecules important for Na^+ channel clustering. The combination of these multiple mechanisms would explain why Na^+ channel cluster abnormalities are more frequent at nodes than at heminodes in the absence of DG (Fig. 2).

Microvillar ERM proteins are reduced in DG-deficient nerves

The first hypothesis is supported by the fact that even mutants for the DG ligand laminin 211 show microvillar and Na^+ channel clustering defects similar to those found in DG-deficient mice (Occhi et al., 2005). Microvillar hypotrophy could be caused by a deficient linkage with ezrin, which is located in microvilli and interacts with β-DG (Spence et al., 2004). In DG-deficient nerves, Western blot revealed a slight decrease in the levels of total and phosphorylated ERMs (Fig. 5 A) after normalization to neurofascin to account for the higher numbers of nodes in mutants caused by short internodes (Court et al., 2009). By

Published February 2, 2015

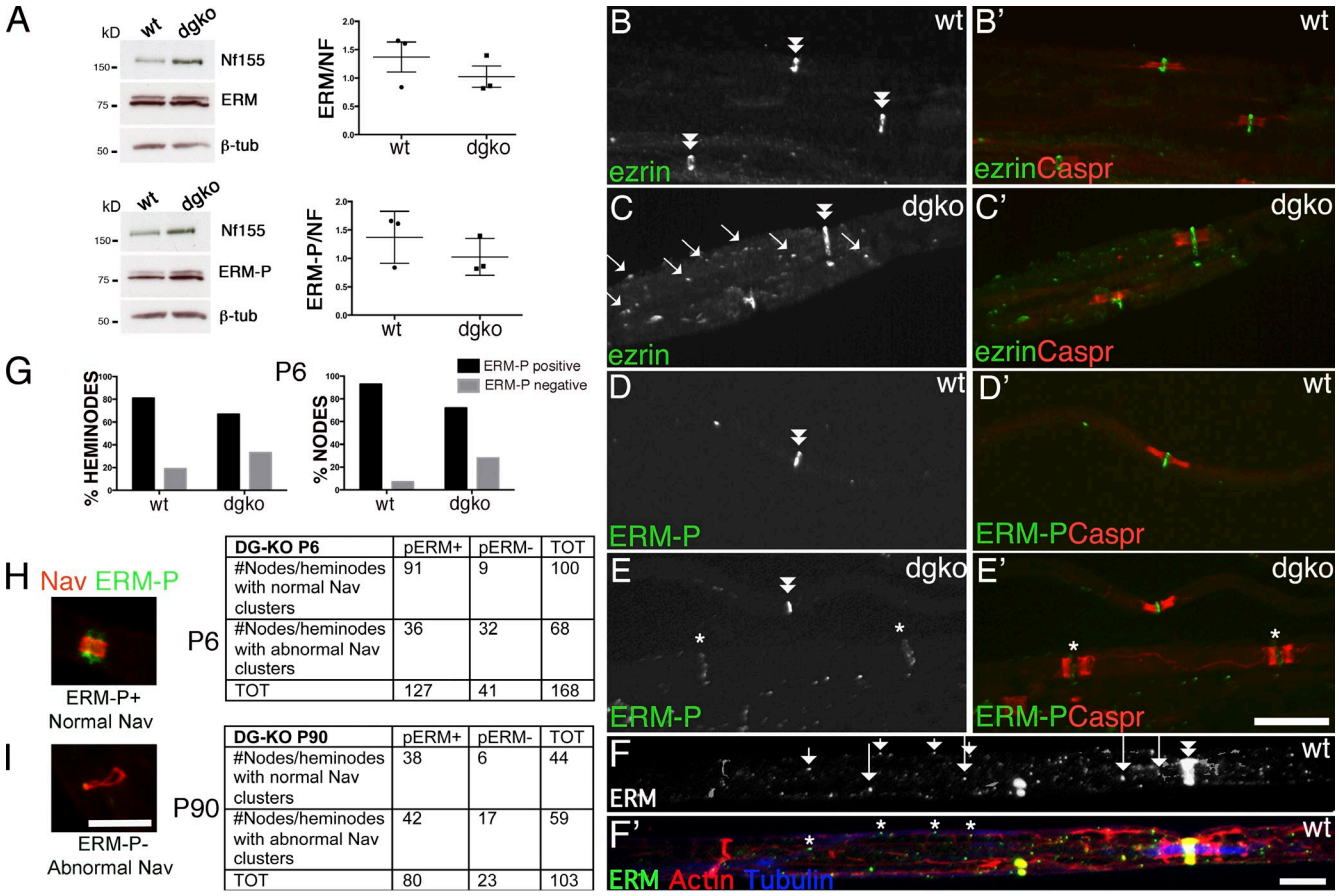

DG-KO P6	pERM+	pERM-	TOT
#Nodes/heminodes with normal Nav clusters	91	9	100
#Nodes/heminodes with abnormal Nav clusters	36	32	68
TOT	127	41	168

P6

DG-KO P90	pERM+	pERM-	TOT
#Nodes/heminodes with normal Nav clusters	38	6	44
#Nodes/heminodes with abnormal Nav clusters	42	17	59
TOT	80	23	103

P90

Figure 5. **Increased internodal and decreased nodal ERM in the absence of DG.** (A) Western blot of sciatic nerve lysates from wild-type and DG-deficient mice, with antibodies against ERM or phophorylated ERM (ERM-P), normalized to NF155. (right) Ratio of ERM/NF155 and ERM-P/NF155 on three mice per genotype; bars represent SEM. Differences are not significant by Student's *t* test. (B–E) Teased fibers from wild-type and dgko adult sciatic nerve immunostained for ezrin (B and C, green), ERM-P (D and E, green), and Caspr (red). (B′–E′) merged images. Note increased ezrin-positive puncta (C, arrows) and lower levels of ERM-P at some dgko nodes (E–E′, asterisks). Double arrowheads indicate nodes with normal amount of ERMs. (G) The percentage of nodes and heminodes (flanked by Caspr) that contain ERM-P were decreased in P6 DG-deficient mice. $n = 3$ mice/genotype; $P < 0.0001$ for nodes and $P < 0.01$ for heminodes by Fisher's test. (H and I) Teased fibers were stained for Nav 1.6 and ERM-P, and the number of normal and abnormal clusters were correlated with ERM-P staining (examples of a normal Nav cluster, ERM positive, and of an abnormal Nav clusters, ERMP negative, are shown) The absence of p-ERM at nodes correlated with abnormal Na^+ channel clusters at P6. $P < 0.0001$ at P6 and $P = 0.09$ at P90 by χ^2 test. (F and F′) ERM (green) puncta (arrows in F and asterisks in F′) in Cajal bands (containing phalloidin-labeled f-actin, red) colocalize with microtubules (stained with tubulin, blue). Bars: (B–E′) 17.5 µm; (F, H, and I) 5 µm.

immunofluorescence, although ezrin is normally restricted to nodes, we observed a higher number of cytoplasmic puncta along the fiber, suggesting an impairment of ERM transport or increased endocytosis (Fig. 5 C, arrows). Indeed, when the image was overexposed, we detected some internodal ERM puncta along microtubules also in normal nerves (Fig. 5 F), suggesting that they may be transported along microtubules in the cytoplasmic channels named Cajal bands (Court et al., 2004). Cajal bands and microtubular tracks are disrupted in SCs lacking laminin 211 and DG (Court et al., 2009), providing a possible common mechanism resulting in impaired ERM transport. Indeed ERM-P nodal staining was frequently reduced in DG-deficient nodes (Fig. 5, E and G). The absence of ERM-P at nodes correlated with Na^+ channel abnormalities at P6, but not at P90 (Fig. 5, H and I). Thus, the absence of DG decreases ERM accumulation in a subset of nodes, and this may contribute to abnormal Na^+ channel clustering during development.

α-DG can be shed after proteolysis cleavage and binds SC and the ECM, but not axons

The second possibility is that DG favors the concentration of molecules that promote Na^+ channel clustering in the nodal gap. This could be mediated by DG directly or by DG ligands HSPGs, which have been proposed to mediate the incorporation of gliomedin into the nodal ECM (Eshed et al., 2007). To address this, we first asked if fragments of the ligand binding α-DG could be released in the nodal gap and if they bound molecules on axons, SCs, or the ECM. Metalloproteinase 2 and 9 cleave β-DG releasing the N-terminal domain of β-DG with α-DG. This cleavage is active and regulated in SCs (Court et al., 2011) and could shed the whole α-DG molecule in the nodal gap. In addition, α-DG is cleaved by a furin protease in cell lines, releasing the N-terminal domain α-DG-N (Singh et al., 2004; Saito et al., 2008). Because gliomedin is also secreted upon furin proprotein convertase cleavage (Eshed et al., 2007; Maertens et al., 2007; Feinberg et al., 2010), we asked if

Published February 2, 2015

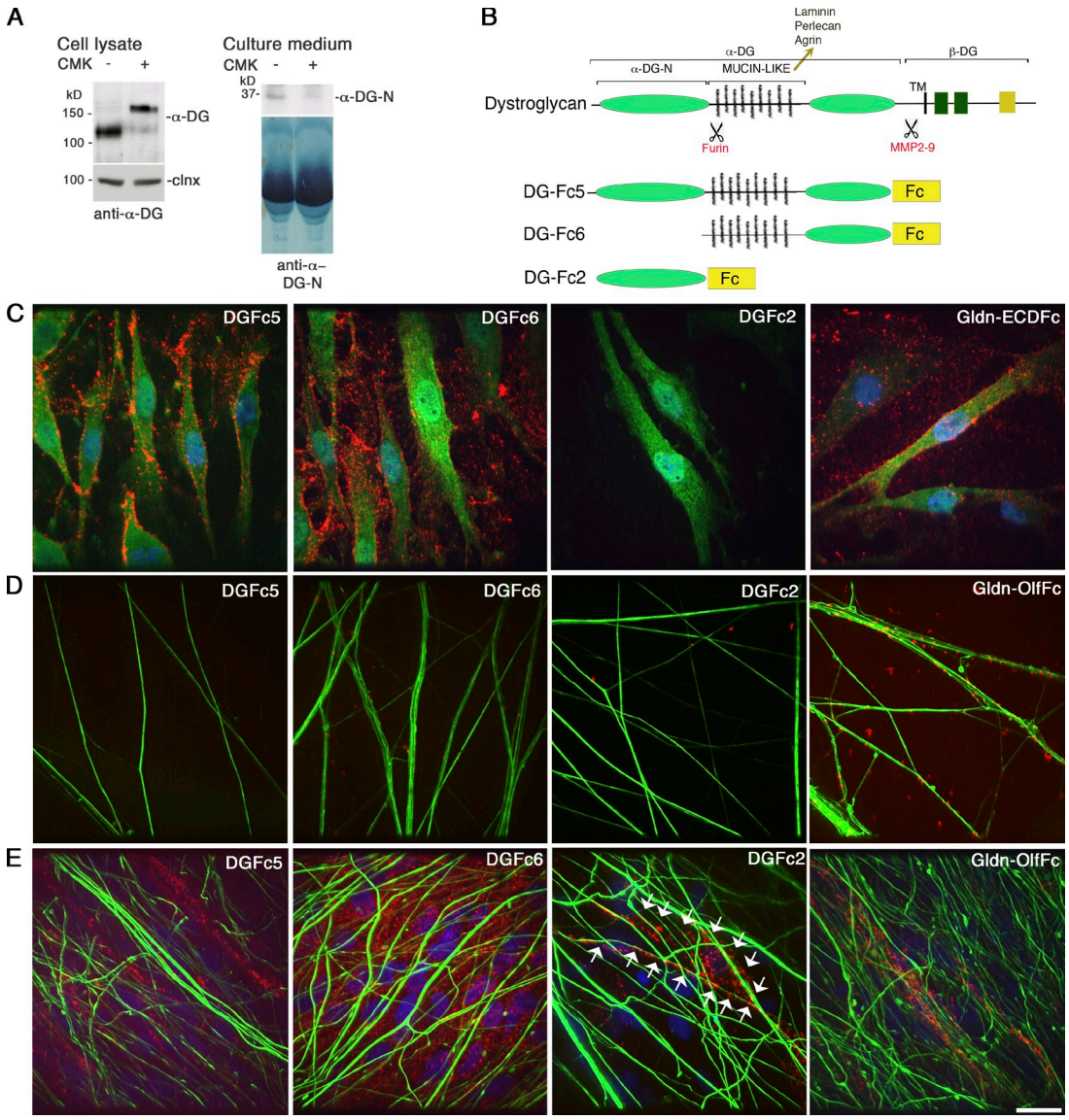

Figure 6. **α-DG fragments can be secreted and bind SCs and the ECM via the mucin-like domain.** (A) Native α-DG-N is cleaved by furin proteases in rat SCs. SCs were cultured with (+) or without (−) furin inhibitor I (CMK). Western blot of SC lysate and culture medium with an anti–α-DG (IIH6) or an anti–α-DG-N antibody shows that α-DG-N is secreted in the medium and a 120-kD α-DG band is in cells. CMK inhibits α-DG cleavage, as shown by the higher molecular mass (160 kD) of α-DG in SCs and absence of α-DG-N in the medium. Calnexin (clnx) is a loading control. (B) Schematic representation of α-DG, showing its domain composition (N-terminal α-DG-N, mucin-like, transmembrane [TM]; sites of furin and MMP cleavage) and of DGFc proteins DGFc5 (whole α-DG-Fc), DGFc6 (deletion of α-DG-N-Fc), and DGFc2 (α-DG-N). (C) Binding of DG-Fc fusion proteins to rat SCs revealed with anti-Fc (red) and anti-S100 (green, SC marker) antibodies. Nuclei are labeled with DAPI (blue). DGFc5 and DGFc6, but not DGFc2, bind to the SC surface and the associated matrix. Gldn-ECDFc binds mainly to the ECM. (D) Binding of Fc fusion proteins to DRG neurons. Only Gldn-OlfFc binds neurons. (E) Binding of DG-Fc fusion proteins to SC-DRG co-cultures after 10 d in myelinating media. Fc binding is in red and neurofilaments are in green. DGFc5 and DGFc6 bind to the ECM and DGFc2 occasionally binds to SCs aligned with axons (arrows). Bar, 17.5 µm.

α-DG-N was released by SCs to potentially be deposited in the nodal gap. Rat SCs cultured in the presence of the furin inhibitor I (CMK) were analyzed by Western blot. In the absence of CMK, α-DG in cell lysates had a molecular weight of ∼120 kD using the IIH6 antibody, which recognizes the mucin-like domain of α-DG, whereas conditioned medium contained an ∼35–40-kD fragment detected by an anti–α-DG-N–specific antibody (Saito et al., 2008; Fig. 6 A). After treatment with CMK the IIH6 antibody detected α-DG with a larger molecular mass of ∼160 kD in cell lysates, whereas the 35–40-kD band became undetectable in culture medium (Fig. 6 A). Finally, treatment of dorsal root ganglia (DRG)/SC co-cultures with CMK inhibited myelination and reduced Na^+ channel clustering at nodes (Fig. S2). Thus α-DG-N is excised by furin and shed, and furin cleavage could control the composition of the nodal gap. To ask if α-DG can bind SC, matrix, or axonal molecules around nodes, we used α-DGFc fusion proteins and performed binding assays. DGFc5 represents the whole α-DG, DGFc6 has a deletion in the N-terminal domain, whereas DGFc2 encompasses the N-terminal domain (Fig. 6 B). In cultured SCs, both DGFc5 and DGFc6, but not DGFc2, bound to the cell membrane and were deposited in the ECM, similar

Published February 2, 2015

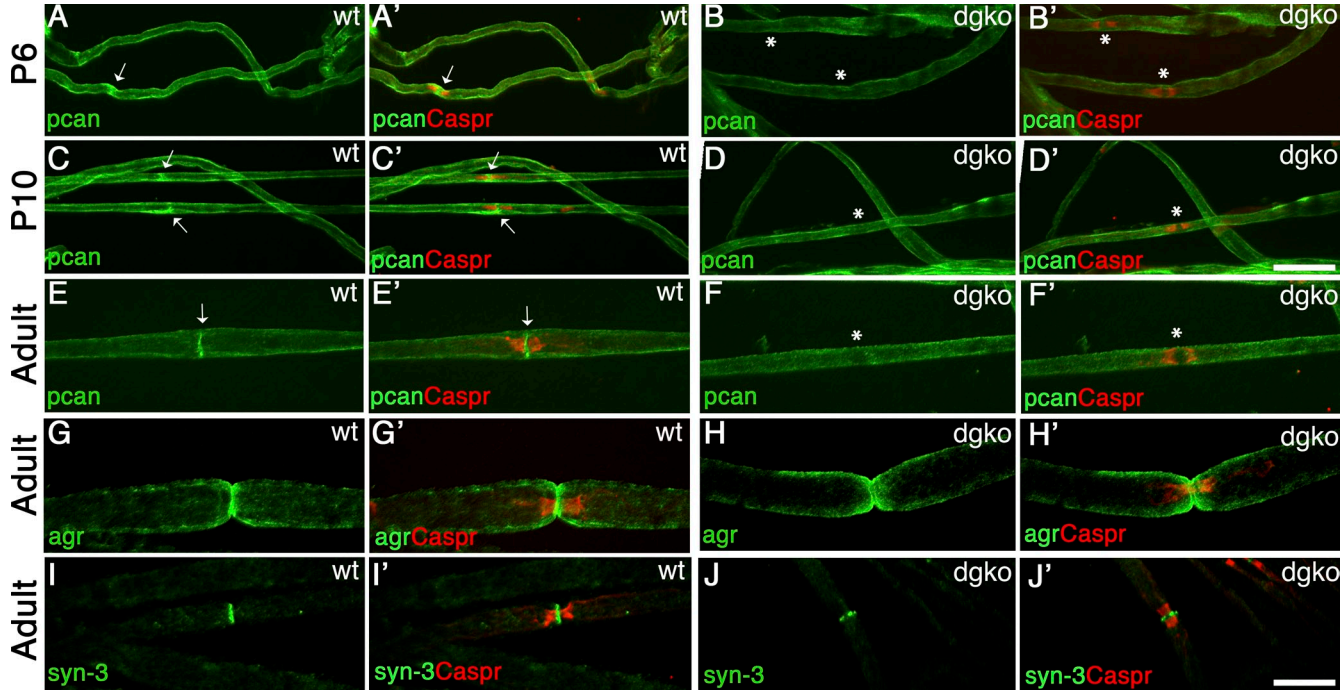

Figure 7. **Perlecan is at nodes of Ranvier and is selectively lost in the absence of DG.** Sciatic nerve fibers from wild-type and dgko mice. Staining for agrin (agr), perlecan (pcan), or syndecan-3 (syn-3; green; A–J) and Caspr (merged confocal images in A′–J′). Perlecan is enriched at wild type developing (A and C) and adult (E) nodes (arrows). In the absence of DG, perlecan is lost at nodes, but not in the basal lamina (B, D, and F, asterisks). 68% and 87% Caspr-positive paranodes flank perlecan-positive nodes at P6 and P10 in wild-type nerves. Only 4% and 6% of nodes are perlecan positive in DG-deficient age-matched animals. (G–J′) Agrin (G and H) and syndecan-3 (I and J) are at nodes, but they are retained in the absence of DG (G′–J′). Bars, 17.5 µm.

to extracellular gliomedin (Gldn-ECDFc; Eshed et al., 2007; Fig. 6 C). Deletion of α-DG-N in the DGFc6 construct did not alter α-DG binding, indicating that the mucin-like and the C-terminal domains of α-DG are sufficient to mediate interaction with SCs. At least qualitatively, more DG-Fc6 than DG-Fc5 attached to the ECM (Fig. 6), possibly indicating an inhibitory role for the α-DG-N fragment. Finally, heparin treatment did not inhibit Fc5 and Fc6 binding to SC and ECM (unpublished data). In contrast to preclustered olfactomedin-Fc (Gldn-OlfFc; Eshed et al., 2005), none of the DG-Fc constructs were able to interact with isolated DRG neurons (Fig. 6 D). Co-culturing of SCs and DRG neurons and inducing myelination did not change the binding of DGFc5 and DGFc6 to SCs and the ECM (Fig. 6 E), but induced occasional binding of DGFc2 to SCs associated with axons, similarly to Gldn-OlfFc (Fig. 6 E). Finally, none of the DGFc constructs bound CHO cells expressing NF186, NrCAM, or gliomedin (unpublished data). Overall, these results suggest that α-DG does not directly interact with axonal or known nodal proteins, but binds SCs and the ECM via the mucin-like domain. This suggests that DG interacts with physiological ligands such as laminin or proteoglycans secreted by SCs and deposited into the nodal gap.

Perlecan is reduced in DG-deficient nodes, but two different perlecan mutants have normal Na^+ channel clusters

We next asked if proteoglycans that are known DG ligands are found at nodes and discovered that the HPSGs agrin and perlecan (Gesemann et al., 1998; Talts et al., 1999) are enriched at nodes of Ranvier (Fig. 7, E–G). Notably, perlecan is absent in the majority of nodes deficient in DG (Fig. 7 F), indicating that DG is required to localize perlecan at nodes. Perlecan is at nodes early in postnatal development (Fig. 7, A–C) and absent in DG-deficient nerves as early as P6 (Fig. 7, B–D), supporting a potential role in the formation of Na^+ channel clusters. To test this, we analyzed peripheral nerves from two different perlecan mutant mice: *Hspg2*$^{\Delta 3/\Delta 3}$, lacking the attachment sites of heparan sulfate (HS) side chains (Rossi et al., 2003), and *Hspg2*$^{KI/KO}$, compound heterozygote carrying a null allele and a point mutation found in Schwartz-Jampel syndrome (Stum et al., 2008; Bangratz et al., 2012), which results in a severe hypomorph. *Hspg2*$^{KI/KO}$ mutants display congenital nerve hyperexcitability and muscle stiffness caused by dysfunction of muscles and neuromuscular junctions (Stum et al., 2008; Bangratz et al., 2012). Clusters of gliomedin and Na^+ channels were not altered in adult *Hspg2*$^{\Delta 3/\Delta 3}$ mice (Fig. 8, A–D) or in developing and adult *Hspg2*$^{KI/KO}$ nodes and heminodes, despite the marked reduction of perlecan in P6 mutant nerves (Fig. 8, E–F′). Overall, these results indicate that DG is required to concentrate perlecan in the nodal gap, but absence of perlecan alone is not sufficient to impair Na^+ channel clustering. Indeed, in addition to perlecan and agrin, syndecan-3 and -4 and versican-1 are present at nodes (Goutebroze et al., 2003; Melendez-Vasquez et al., 2005), and their localization at nodes is maintained in the absence of DG and perlecan (Fig. 7, H and J; and Fig. S3). Thus, it is probable that significant redundancy among proteoglycans exists in PNS nodes, similar to a recent study in the CNS (Susuki et al., 2013).

Published February 2, 2015

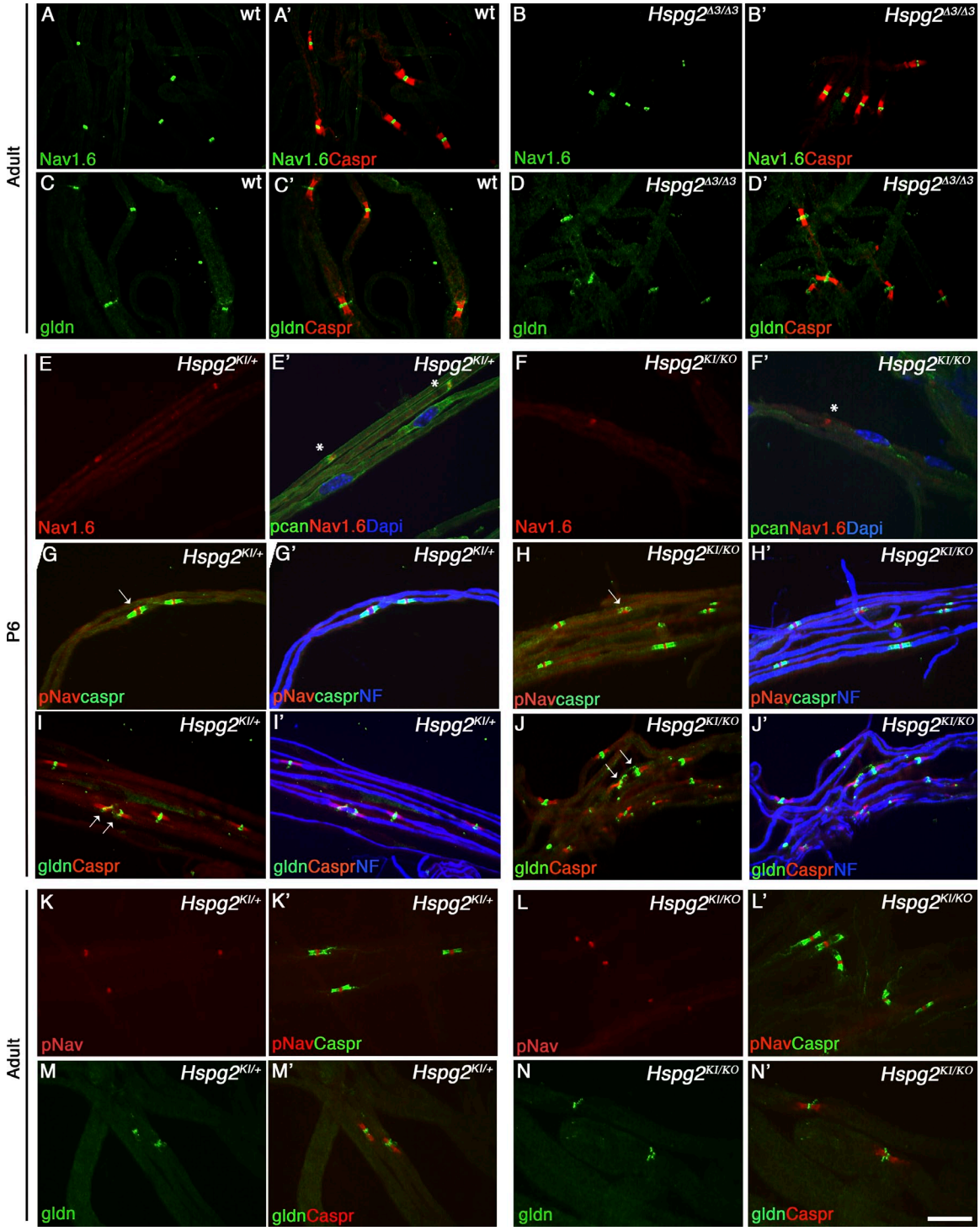

Figure 8. **Na^+ channel clusters are retained at nodes or heminodes of two different perlecan mutants.** (A–D) Sciatic nerve fibers from adult wild-type (A and C) and *Hspg2*$^{\Delta3/\Delta3}$ (B and D) mice. Immunostaining for Na^+ channel 1.6 (A and B, green), gliomedin (C and D, green), and Caspr (A′–D′, red) shows no alterations in nodal clusters. (E–N) Sciatic nerve teased fibers from P6 (E–J) or adult (K–N) *Hspg2*$^{KI/+}$ (controls) and hypomorphic *Hspg2*$^{KI/KO}$ mice. Staining for Na^+ channel 1.6 (E and F, red) and perlecan (E′ and F′, green). Perlecan is enriched at nodes of controls (E′, asterisks), but its expression is almost absent in *Hspg2*$^{KI/KO}$ nerves and nodes (F′, asterisk). Immunostaining for pan-Na^+ channel (G, H, K, and L, red) and Caspr (G′, H′, K′, and L′, green) or gliomedin (I, J, M, and N, green) and Caspr (I′ and J′, red) show normal accumulation of gliomedin and formation of clusters at heminodes (I and J, arrows) and nodes (G and H, arrows) in perlecan hypomorphs. NF, neurofilament (blue). Bar, 17.5 µm.

Perlecan binds gliomedin and favors Na^+ channel cluster formation

It was recently reported that the proteoglycans versican2, brevican, and Bral1 stabilize Na^+ channels at CNS nodes by binding to NF186 and Na^+ channels (Hedstrom et al., 2007; Susuki et al., 2013). We thus assessed whether perlecan also binds NF186 or other nodal components. Recombinant perlecan was purified (Fig. 9 A) and spotted at increasing concentrations for Far

Published February 2, 2015

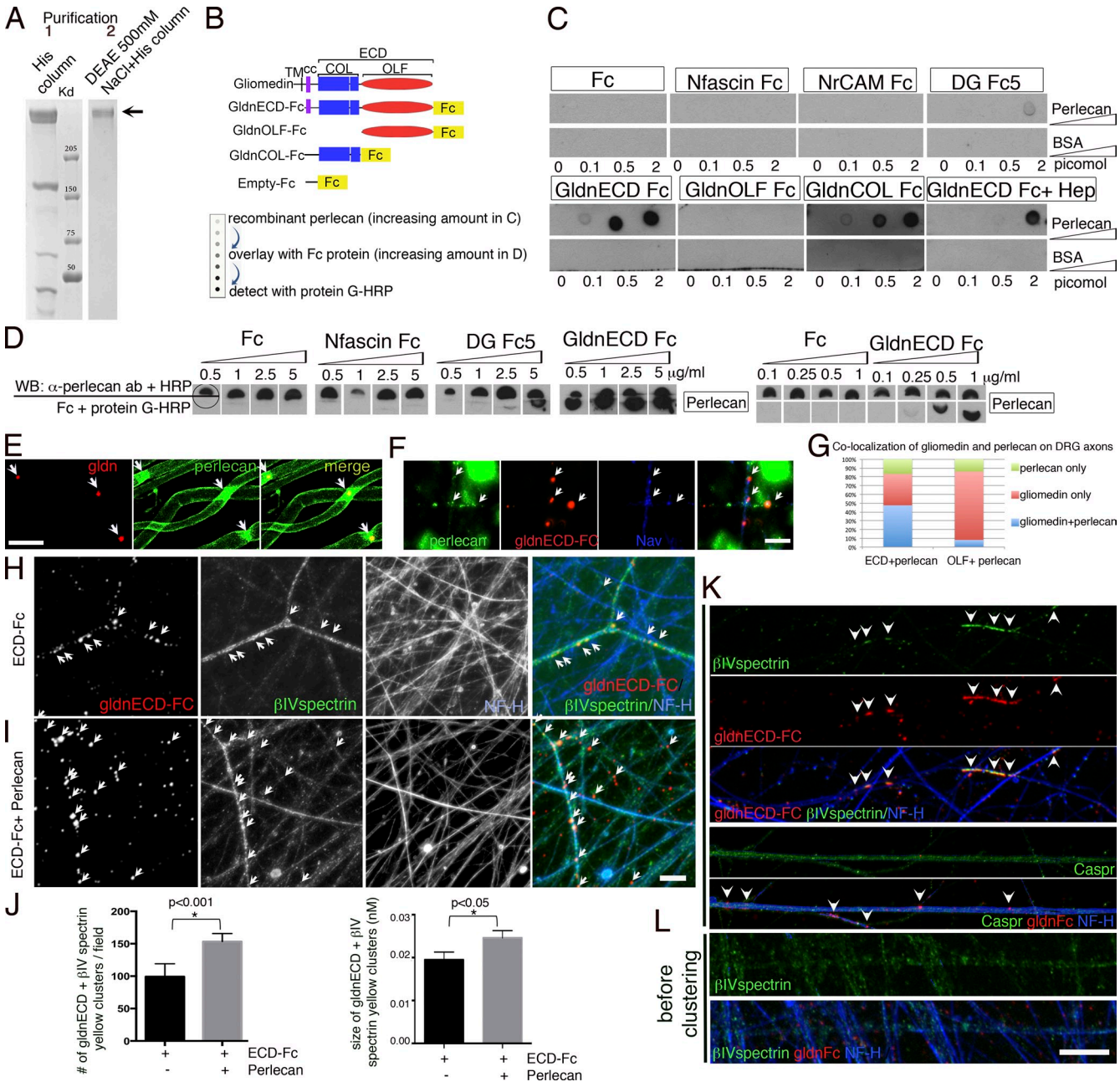

Figure 9. **Perlecan binds the collagen domain of gliomedin and increases gliomedin binding to axons and formation of Na^+ channel clusters.** (A) Comassie blue staining of recombinant perlecan after the first and second step of purification (1 and 2) shows a single band of high molecular mass, consistent with the predicted size of perlecan (arrow). (B) Gliomedin-Fc fusion proteins and Far Western strategy. The whole extracellular domains of NF186, NrCAM, and DG were also used as fusion proteins. (C) Spotting increasing concentration of perlecan shows that only DG and gliomedin, via the collagen domain, bind perlecan. Addition of heparin inhibits the binding. (D) Spotting constant amounts of perlecan (0.5 pM) and overlying increasing amounts of purified Fc-fusion proteins shows that perlecan binding to gliomedin is dose dependent. To confirm equal loading, filters containing the perlecan spot were cut in two and the top half was hybridized with anti-perlecan antibodies. (E) Adult teased fibers from sciatic nerves stained for gliomedin (red) and perlecan (green) show that the two molecules colocalize at nodes (arrows). (F, H, and K) Nodal clustering was induced on DRG neurons by preclustered Fc-gliomedin (gldn) ECD or OLF. Staining of gliomedin clusters (arrows) with anti-Fc antibodies (red) shows that they contain Na^+ channels (F, blue), βIV spectrin (H, I, and K, green), and perlecan (F, green). Perlecan colocalized more frequently with Gldn-ECD clusters than Gldn-OLF clusters (G). $n = 585$ from a single experiment. (H and I) Perlecan increases Gldn ECD-Fc binding to neurons and formation of clusters that contained gldnECD and βIV spectrin (arrows). Neurons are stained with neurofilament (cyan). (J) The number and size of clusters containing gldnECD and βIV spectrin per field of view from six coverslips and two independent experiments were counted; $n = 29$ fields. Bars represent SEM and statistical significance was evaluated by Student's *t* test. (K) Gldn-Fc induced clusters (arrowheads) that co-clustered with βIV spectrin, but not with the transmembrane paranodal protein Caspr. (L) βIV spectrin was diffuse along axons before clustering. Bars: (F, H, I, K, and L) 5 µM; (E) 10 µM.

Western assay. The membrane was overlaid with recombinant Fc fusion proteins for the extracellular domains of neurofascin, NrCAM, gliomedin (ECD-Fc), or α-DG (DG-Fc5) and binding was revealed. As predicted, the positive control α-DG bound to perlecan, whereas empty Fc did not bind. In addition, gliomedin ECD-Fc bound strongly to perlecan (Fig. 9 C).

Published February 2, 2015

In contrast, and differently from CNS proteoglycans, we could not detect binding of NF186 or NrCAM to perlecan. It was shown that gliomedin ECD-Fc induces Na^+ channel clustering on isolated DRG neurons, provided that the Fc domain is preaggregated with anti-Fc antibodies (Eshed et al., 2005). Gliomedin ECD contains two domains that are both required to cluster nodal proteins: the olfactomedin domain (OLF), which binds NF186 and NrCAM; and the collagen-like domain that mediates multimerization and incorporation into the ECM by binding to HSPGs (Eshed et al., 2007; Labasque et al., 2011). We postulated that perlecan could be one of the HSPGs that incorporates gliomedin into the ECM. To test this, we first asked if deletion of either the olfactomedin or the collagen-like domain prevented binding to perlecan, and found that indeed the collagen domain of gliomedin was necessary and sufficient (Fig. 9, B and C). Finally the HS chains of perlecan contributed binding, because binding was reduced in the presence of heparin (Fig. 9 C). Treatment of perlecan with heparinase descreased, but not abolished binding (Fig. S4), indicating that gliomedin binds to both the perlecan protein core and HS chains. We next repeated the Far Western by spotting constant amounts of perlecan and overlaying increasing amounts of purified Fc fusion proteins. As shown in Fig. 9 D, perlecan bound gliomedin in a dose-dependent fashion and with higher affinity than DG. Solid-phase assay experiments predict apparent dissociation constants of 8 nM for gliomedin and 41 nM for DG (Fig. S4). Next, we confirmed that perlecan and gliomedin colocalize at nodes of Ranvier in teased fibers in vivo (Fig. 9 E). Finally, we asked if the addition of recombinant perlecan to DRG treated with gliomedin Fc influenced gliomedin binding to neurons and the clustering of nodal components. Strikingly, perlecan increased the formation of nodal-like gliomedin clusters that contained βIV spectrin (Fig. 9, H–J). Binding of gliomedin Fc and cluster formation was specific, because Fc alone did not bind, irrespective of the presence of perlecan (unpublished data). Na^+ channels and βIV spectrin, but not Caspr coclustered with gliomedin (Fig. 9, F and K) and BIV spectrin was diffusely localized along axons before clustering (Fig. 9 L). Perlecan localized to clusters and colocalized with Gldn-ECD, but not with Gldn-OLF (Fig. 9, F and G). Addition of perlecan alone did not induce Na^+ clustering (unpublished data). As expected, the collagen-like domain of gliomedin alone was not able to induce Na^+ channel clustering, with or without perlecan (unpublished data). These data show that perlecan is one HSPG that favors binding of gliomedin to axons and formation of nodal-like clusters, possibly by optimizing gliomedin multimerization and presentation to NrCAM and NF186.

Discussion

Multiple mechanisms underlie the formation of nodes of Ranvier and adjacent paranodes and juxtaparanodes. One is incorporation of gliomedin in the perinodal gap, where it is postulated to interact with proteoglycans and to form a net that favors clustering of Na^+ channels. Here we show that perlecan is the proteoglycan that interacts with gliomedin at nodes and favors gliomedin binding to axons and clustering of Na^+ channels. We also show that DG favors the initial events of node formation by recruiting perlecan and organizing the SC cytoskeleton in microvilli. Multiple proteoglycans are redundant in PNS nodes (Melendez-Vasquez et al., 2005; this paper). This is reminiscent to what was recently described in CNS nodes (Susuki et al., 2013), although a different set of molecules are used.

DG participates in the initial events of nodes of Ranvier formation

DG and laminins are required for proper clustering of Na^+ channels at PNS nodes. Specific laminins (211 and 511) and dystrophin complexes (Dp116) localize at nodes (Occhi et al., 2005), suggesting that a unique basal lamina–cytoskeletal linkage promotes nodal architecture. Our data exclude that laminin 511 participates in node formation because it localizes over nodes after they are formed. In contrast, Na^+ channels cluster abnormally at nodes and heminodes in the absence of DG, suggesting that DG is involved in the formation of Na^+ channel clusters.

DG helps Na^+ channel clustering via two distinct mechanisms

Our data suggest two nonmutually exclusive mechanisms by which DG favors nodal Na^+ channel clustering (Fig. 10): a canonical interaction with the ECM organized in the basal lamina above nodes (i.e., laminin 211); and a non-canonical interaction with amorphous ECM in the nodal gap (i.e., perlecan). In the first case, DG may influence the architecture of the node indirectly by regulating transport in Cajal bands and organization of ERM proteins in the microvilli cytoskeleton. In the second instance, DG is required locally to retain perlecan at nodes.

Microvilli, Cajal band transport, and nodes of Ranvier

DG and its dystrophin partners' utrophin and DRP2/Periaxin are crucial for the organization of internodes by regulating Cajal band formation and internodal length (Court et al., 2004, 2009). Cajal bands probably endow the extremely long myelinating cell with specialized cytoplasmic channels in which microtubule-mediated transport of molecules and organelles is optimized (Court et al., 2004, 2009). In support of this, DG-null internodes contain numerous ERM puncta along microtubule tracks, suggesting that ERM transport to microvilli is impaired. We postulate that this may cause microvilli to be hypotrophic in DG nodes. Similarly, because DG-deficient internodes are short, it is conceivable that paranodes exert less mechanical force to fuse heminodal clusters into nodes.

Perlecan, gliomedin, and clustering of Na^+ channels

Growing evidence shows a direct effect of the ECM, such as perineuronal nets and the nodal substance, on neuronal function (Kwok et al., 2011). The nodal gap ECM, earlier termed "cementing disc of Ranvier," contains proteoglycans and non-sulfated mucopolysaccharides (Hess and Young, 1952; Landon and Langley, 1971) and is emerging as a region of communication between glia and the axolemma critical for Na^+ channel clustering. In the PNS, gliomedin binds NF186 when shed into

Published February 2, 2015

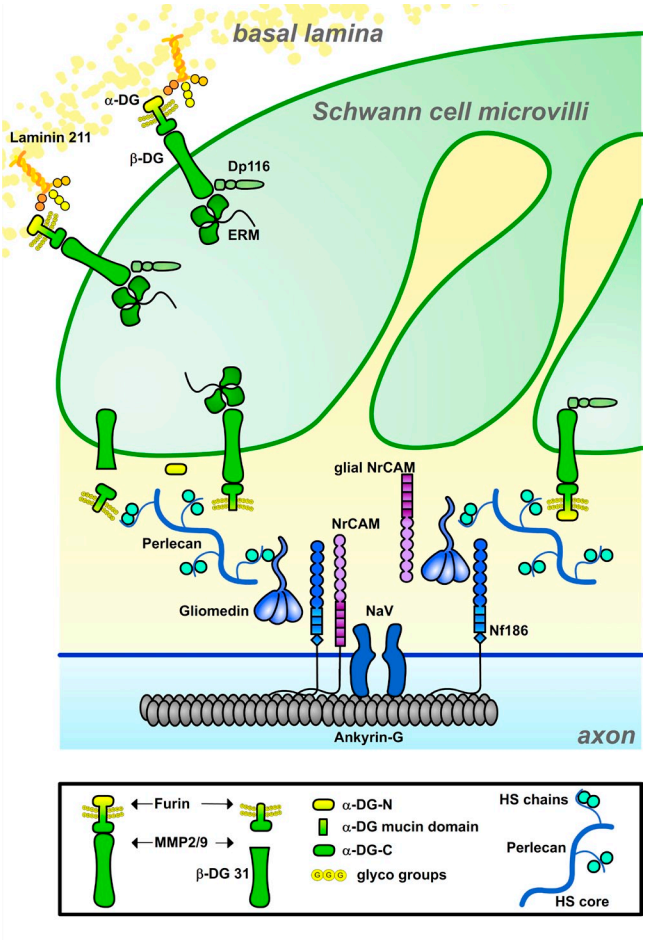

Figure 10. **Model for DG and perlecan participation in Na^+ channel clustering at nodes.** DG aids axonal Na^+ channel clustering via different, not mutually exclusive, mechanisms. At the side of basal lamina, DG interaction with laminin 211 regulates the formation of Cajals bands, which may favor ERM transport and remodeling of the microvilli. In the nodal gap, α-DG retains perlecan, which binds gliomedin and favors its binding to axons. It is not known if α-DG at nodes is anchored to the membrane of microvilli or released after cleavage by furin or metalloproteinases. It is possible that two sequential cleavages, by MMPs and furin, release two forms of α-DG with distinct functions in Na^+ channel clustering.

the nodal matrix and incorporated in a multimolecular complex in an HS-dependent manner (Eshed et al., 2007). Here we show that perlecan is retained by DG in the nodal gap and binds the collagen domain of gliomedin, possibly contributing to its polymerization. This interaction is through the core protein but impaired by heparin, suggesting that the HS chains of perlecan modulate the interactions of gliomedin with the nodal ECM. This in turn is needed to favor binding of the olfactomedin domain to NF186. In nerves mutant for perlecan, gliomedin and Na^+ channels were still localized at nodes, suggesting that perlecan is not the only HPSG interacting with gliomedin. Other HSPGs may be redundant with perlecan in modulating the binding of gliomedin to the ECM or to axons. The function of perlecan at nodes resembles that of HSPGs in other locations, which trap growth factors to prevent proteolysis, favor high-affinity receptor binding, or modulate release and bioavailability (Bishop et al., 2007; Bix and Iozzo, 2008). However, not all roles of perlecan are mediated by growth factors. Perlecan binds other molecules, including ECM components like collagens, via either the HS or the core protein (Whitelock et al., 2008; Farach-Carson et al., 2014). In PNS nodes, our data suggest that the interaction between perlecan and collagens (gliomedin) favors Na^+ channel clustering.

Similarities and differences between CNS and PNS nodes

Our data reveal that SCs and central glia use similar strategies at nodes, in that both adopt a set of proteoglycans to form a functionally redundant network that ensures formation and maintenance of high Na^+ channel density. However, the specific set of proteoglycans used is different, probably reflecting the differing cellular origin of the matrix and the lack of basal lamina in CNS myelin.

In contrast to the HSPG perlecan, CNS nodes rely on chondroitin-sulfate proteoglycans and hyaluronan-binding and linker proteins: versican V2, brevican, neurocan, phosphacan, and Bral1 (Melendez-Vasquez et al., 2005; Hedstrom et al., 2007; Dours-Zimmermann et al., 2009; Bekku et al., 2010). Similar to perlecan, genetic loss of single CNS proteoglycans does not affect clustering of Na^+ channels, although ionic diffusion, buffering, and conduction velocity may be affected (Weber et al., 1999; Brakebusch et al., 2002; Dours-Zimmermann et al., 2009; Bekku et al., 2010). A core of proteoglycans (brevican, versican V2, and Bral1) maintains localization of the others and interacts with NF186 (Dours-Zimmermann et al., 2009; Bekku et al., 2010; Susuki et al., 2013). Deletion of these core proteins plus another redundant mechanism (i.e., paranodal or nodal adhesion molecules) prevents Na^+ channel clustering (Susuki et al., 2013). The function of perlecan in the PNS and of these core CNS proteoglycans appears different. CNS proteoglycans bind NF186 and can initiate Na^+ channel clustering, but are accumulated at nodes after Na^+ channels are clustered, similar to laminin 511 in PNS nodes, and are therefore considered stabilizers of nodes (Susuki et al., 2013). In contrast, PNS perlecan does not bind NF186, but is localized early at nodes and may participate in the initial phases of clustering by favoring incorporation of gliomedin into the matrix.

Despite these differences there are also similarities. For example, perlecan, gliomedin, agrin, and other HSPGs are secreted by oligodendrocytes or astrocytes and some accumulate at nodes (Kaplan et al., 2001; Winkler et al., 2002; Eshed et al., 2007). When astrocytes or oligodendrocytes are analyzed separately in culture, they show similarities and differences from SCs at nodes. For example, oligodendrocytes secrete a Na^+ channel clustering activity, which remains elusive (Kaplan et al., 1997). However gliomedin binds the ECM produced by SCs, but not that of astrocytes (Eshed et al., 2007). Assuming that SCs perform the role of both oligodendrocytes and astrocytes at paranodes and nodes, it is possible that similar experiments conducted with oligodendrocytes and astrocytes together may reveal that a combination of molecules secreted by oligodendrocytes (e.g., an HSPG fragment) and astrocytes (e.g., gliomedin) accounts for the elusive oligodendrocyte-secreted clustering activity (Kaplan et al., 1997).

Published February 2, 2015

Thus, the question remains whether an equivalent set of ECM components that function in both initiation and stabilization of Na^+ channel clusters exist at CNS and PNS nodes, or if the simpler PNS combines the multiple functions performed in the CNS by astrocytes and oligodendrocytes into SCs, which use only a restricted set of molecules.

Materials and methods

Mice

The generation of transgenic and knockout mice was previously described (Moore et al., 2002). In brief, the *Dag1* floxed allele was created using a targeting construct with a floxed PGK-neo vector that resulted in the insertion of a floxed neomycin (neo) cassette at the SalI site in intron 5′ of exon 2 and a loxP site at an EcoRV site 3′ of exon 2 of mouse *Dag1* (a gift from K. Campbell, University of Iowa, Iowa City, IA; Moore et al., 2002). P0Cre mice were generated using the mP_0TOTA(Cre) transgene, which contains a 1.1-kb segment of the gene encoding Cre recombinase under the control of a complete mouse *Mpz* gene with 6 kb of promoter, all exons and introns, and a natural polyadenylation site (Feltri et al., 1999). *Caspr* null mice (*caspr*$^{-/-}$) were derived using a replacement-type vector in which a neo resistance gene replaces an SphI–BssHII fragment containing *Caspr* exon 1, including the initiator methionine and the signal sequence (Gollan et al., 2003). *Hspg2*$^{\Delta 3/\Delta 3}$ mice were generated using a targeting construct that replaces a 130-bp KpnI–BamHI fragment containing *Hspg2* exon 3 with a PGK neo cassette (Rossi et al., 2003). The *Hspg2*^{KI} allele was generated by introducing the c.4595G.A (p.C1532Y) point mutation into exon 36 and a floxed PGK neo cassette containing a polyadenylation signal into intron 36 in the same orientation as *Hspg2*, 86 bps downstream from exon 36 (Stum et al., 2008; Bangratz et al., 2012). The *Hspg2*^{KO} allele was produced using a gene-trapping strategy (Skarnes et al., 1995), which results in a fusion protein between truncated perlecan and LacZ, retained within the ER. These mice do not have detectable perlecan mRNA and they are phenotypically similar to perlecan-deficient mice described by Arikawa-Hirasawa et al. (1999). Mice lacking DG specifically in SCs, *dag1*$^{flox/flox}$//P0Cre (referred to as dgko), were described previously (Saito et al., 2003; Occhi et al., 2005) and were congenic in C57BL6/N. *Caspr* null mice were congenic in ICR. Double mutant dgko//*Caspr*$^{-/-}$ mice were obtained by crossing heterozygous *Caspr*$^{+/-}$ with *dag1*$^{flox/flox}$//P0Cre and intercrossing *dag1*$^{flox/+}$//P0Cre//*Caspr*$^{+/-}$. Double knockouts were obtained with Mendelian ratio. *Hspg2*$^{KI/+}$ and *Hspg2*$^{KO/+}$ mice were on DBA/2J and C57Bl6 background, respectively. The analysis of *Hspg2*$^{KI/KO}$ mice was performed on a mixed DBA/2J//C57Bl6 background. Spraw-Dawley rats were used for in vitro experiments. All experiments involving animals were performed according to protocols approved by San Raffaele Hospital and University at Buffalo Institutional Animal Care and Use Committee and complied with National Institutes of Health guidelines.

Antibodies

Primary antibodies included the following: rabbit anti-Caspr (6061; 1:800), mouse anti-Caspr (M275; 1:1), rabbit anti-olfactomedin (Ab320; 1:1,000), rabbit (Ab720; 1:200) and mouse anti-gliomedin (Mab94; 1:50; Eshed et al., 2005, 2007), mouse anti–β-DG (43DAG/8D5; Novocastra; 1:50 for IF; 1:80 for WB; 1:1 for IEM), mouse anti-glycosylated α-DG (IIH6; 1:100 for IF; 1:1,000 for WB; 1:100 for IEM; EMD Millipore), rabbit anti–α-DG-N (APl528; 1:70; gift from F. Saito, Teikyo University, Tokyo, Japan), mouse anti-Dp116 (Mandra1; Sigma-Aldrich), rabbit anti-ezrin (EMD Millipore), rabbit anti-ERM and rabbit anti–ERM-P (Cell Signaling Technology), mouse anti-Nav pan (K58/35; Sigma-Aldrich), rabbit anti-Nav1.6 (gift from J. Trimmer, University of California, Davis, Davis, CA), rabbit anti-agrin (AS204; gift from M. Ruegg, Biozentrum, University of Basel, Basel, Switzerland), rabbit anti–versican-1 (gift from D. Zimmermann, University Hospital Zurich, Zurich, Switzerland), rat anti-perlecan (A7L6; EMD Millipore), rabbit anti-perlecan (Handler et al., 1997), rabbit anti-syndecan-3 (Abcam), rat anti-neurofilament-H (gift from V. Lee, University of Pennsylvania, Philadelphia, PA), rabbit anti-S100 (Dako), rabbit anti-neurofascin pan (NFC2199; gift of P.J. Brophy, University of Edinburgh, Edinburgh, UK), rabbit anti-neurofascin and rabbit anti-βIV spectrin (gift of M. Rasband, Baylor College, Waco, TX), mouse anti–β-tubulin (Sigma-Aldrich), rabbit anti-calnexin (Sigma-Aldrich), and rabbit anti-laminin α5 (gift from L. Sorokin, University of Muenster, Muenster, Germany). Secondary antibodies included the following: donkey anti–rabbit FITC, goat anti–rabbit DyLight488, donkey anti–rat FITC, goat anti–rat Cy5 and goat anti–human IgGFc-specific rhodamine (Jackson ImmunoResearch Laboratories, Inc.), goat anti–mouse TRITC and goat anti–mouse IgG2a-specific FITC (SouthernBiotech), goat anti–mouse IgM TRITC (Nordic), goat anti–mouse IgGFab-specific or goat anti–mouse IgGFc-specific HRP (Sigma-Aldrich), and goat anti–rabbit HRP. Anti–mouse 10-nm gold particle–conjugated secondary antibody was used in IEM (British BioCell). Nuclei were stained with DAPI (Sigma-Aldrich).

SDS-PAGE for Perlecan

Perlecan samples were analyzed in 3.5% acrylamide gels under nonreducing conditions and stained with Coomassie blue.

Western blot analysis

Sciatic nerves were dissected from rats or mice, frozen and homogenized in a metal pestle, and then lysed with lysis buffer containing 25 mM Tris, pH 7.4, 95 mM NaCl, 10 mM EDTA, pH 8, 2% SDS, 1 mM NaF, 1 mM Na_3VO_4, and 1% protease inhibitor cocktail (Sigma-Aldrich). After rocking at 4°C for 30 min, samples were spun at 13,200 rpm in a microcentrifuge for 10 min to eliminate insoluble material. The supernatant was recovered and stored at −80°C until use. Protein concentration was determined by BCA protein assay kit (Thermo Fisher Scientific) according to the manufacturer's instructions. Equal amounts of homogenates (containing 5–30 µg of protein) were added to reducing sample buffer (150 mM Tris-HCl, pH 6.8, 6% SDS, 0.3% bromophenol blue, 30% glycerol, and 0.08 M DTT). The samples were denatured, resolved on 5–12% SDS–polyacrylamide gels, and electroblotted onto a polyvinylidene fluoride microporous membrane (PerkinElmer). Membranes were stained with Ponceau red to verify equal loading of proteins. Blots were blocked with 0.1% Tween and 5% dry milk in PBS and incubated with the appropriate antibody in 0.1% Tween and 1% dry milk in PBS. HRP-conjugated secondary antibodies were visualized using the ECL method with autoradiography films (GE Healthcare).

Immunohistochemistry on teased nerve fibers

Teased nerve fibers from sciatic nerves were prepared and immunostained as previously described (Occhi et al., 2005). In brief, nerves from mutant and control mice were dissected and either fixed by immersion in ice-cold 4% paraformaldehyde for 30 min and stored in PBS at 4°C until teasing or washed in PBS and teased immediately. After perineurium removal, nerve fibers were gently separated with tungsten pins (Fine Science Tools) and transferred onto 3-aminopropyltriethoxy-sylane–treated slides. For immunostaining, fibers were permeabilized in cold acetone for 5–10 min at −20°C. After blocking with 5% fish skin gelatin and 0.5% Triton X-100 in PBS, fibers were labeled with primary antibodies, followed by appropriate secondary antibodies, washed, dried, and mounted with Vectashield (Vector Laboratories). Nonspecific background staining was determined when possible by staining tissues deficient in the target protein and in every experiment by omitting the primary antibody.

EM and IEM

EM was performed as previously described (Occhi et al., 2005). For IEM, adult wild-type and DG-deficient mice (used as negative controls) were anaesthetized and perfused with 4% paraformaldehyde/0.05% glutaraldehyde in 0.01 M Na^+ periodate, 0.1 M lysine, and 3% sucrose in 0.1 M phosphate buffer (P/S), pH 7.4. Sciatic nerves were further fixed for 2 h at room temperature, left overnight in 3.5% sucrose in 0.1 M phosphate buffer P/S at 4°C, and then dissected. Tissues were stained with 0.25% tannic acid in P/S for 1 h, washed in P/S, quenched in 50 mM NH_4Cl in P/S, washed in 4% sucrose in 0.1 M maleate buffer, pH 6.2, and incubated for 1 h with 2% uranyl acetate in 0.1 M maleate buffer/4% sucrose (all steps at 4°C). Nerves were dehydrated in 50% (30 min at 4°C), 70%, and 90% ethanol (45 min at −20°C). Tissues were infiltrated at −20°C with LRGold resin (Polysciences)/ethanol (1:1 ratio; 7:3 ratio; 100% LRGold resin; 1 h each), and left in 100% LRGold resin overnight at −20°C. Next, tissues were infiltrated in fresh LRGold resin with 0.5% benzoin methyl ether, first for 1 h and then overnight, embedded in gelatin capsules, and polymerized by UV irradiation (365 nm) for 48 h at −20°C. Sections were collected on nickel formward/carbon grids and treated differently for staining for α- or β-DG. Immunostaing for β-DG was performed using mouse anti–β-DG (Novocastra). Grids were washed twice in PBS, blocked with 0.25% fish skin gelatin and 0.1% Triton X-100 in PBS for 1 h at room temperature, incubated overnight at 4°C with antibodies, rinsed with PBS, and incubated for 1 h with goat anti–mouse antibody conjugated with 10-nm gold particles (British BioCell). Sections were then washed with PBS and distilled water. Staining α-DG was performed using mouse anti-glycosylated α-DG (IIH6) according to Nico et al. (2010). In brief, grids

Published February 2, 2015

were first incubated with TBS buffer for 10 min at room temperature, and then treated with 0.1% trypsin in TBS, pH 7.0, for 4 min. Next, grids were rinsed with TBS, blocked with 1% BSA in TBS, pH 7.4, for 10 min at room temperature, and incubated overnight with primary mouse anti-DG antibody at room temperature. The next day, grids were washed with TBS and incubated for 1 h with secondary antibodies (goat anti–mouse IgM coupled to 10-nm gold particles). Finally, grids were counterstained with saturated uranil acetate and lead citrate. Images were acquired using a transmission electron microscope (912AB; Carl Zeiss).

SC cultures

SCs were isolated from the sciatic nerves of 3-d-old Sprague-Dawley rats and cultured as previously described (Feltri et al., 1992, 1994). In brief, sciatic nerves were dissected and dissociated in 1% collagenase and 2.5% trypsin. Pelleted cells were plated on 100-mm^2 tissue culture plates coated with poly-L-lysine, in DMEM, supplemented with 10% heat-inactivated fetal calf serum, 2 mM L-glutamine, 2 µM forskolin, and 2 ng/ml β-neuregulin-1. Fibroblast growth was inhibited using 10-µM Ara-C, and by complement killing using anti-Thy1.1 antibodies (MCA04G; Serotec) and 400 µl of rabbit complement (234400; EMD Millipore). The cells were re-fed every 3–4 d and subcultured every 7 d. For pharmacological treatment, SCs were plated at 35×10^4 on poly-L-lysine–coated 6-well plates and treated with 20 µM Furin inhibitor I (Dec-RVKR-CMK; EMD Millipore) for 48 h. Cells were next stained or scraped and proteins were extracted on ice with lysis buffer as described in the Western blot analysis section.

Organotypic neuron/SC co-cultures

DRG were isolated after dissecting the spinal cord and associated ganglia of E15.5 rat embryos and dissociated in 0.25% Trypsin solution (Gibco) for 45 min at 37°C. Trypsin was inactivated with FBS (Gibco) and DRGs were resuspended in C-medium, consisting of MEM (Gibco), 2 mM L-glutamine (Gibco), 10% FBS, 4 mg/ml D-glucose (Sigma-Aldrich), 50 ng/ml NGF (Harlan Laboratories, Inc.), and penicillin/streptomycin (Gibco). One or two DRGs were seeded in coverslips coated with collagen in a drop of C-medium (MEM, 4 g/l D-glucose, 10% FBS, 2 mM L-glutamine, and 50 ng/ml NGF) plus 100 U/ml penicillin/100 µg/ml streptomycin for one night. The next day, the C-medium was replaced with NB medium (Neurobasal, 4 g/l D-glucose, 2 mM L-glutamine, 50 ng/ml NGF, and B27 supplement 1×). After one week, myelination was induced with 50 µg/ml ascorbic acid (Sigma-Aldrich). DRG neurons were maintained for 8–10 d with ascorbic acid before being processed for binding experiments and immunofluorescence. To obtain purified DRG neurons, dissociated DRGs were seeded at a density of one DRG per coverslip onto 12-mm coverslips coated with 0.4 mg/ml matrigel (BD) and 100 µg/ml poly-L-lysine (Sigma-Aldrich) and incubated at 37°C with 5% CO_2. After 24 h the medium was changed and purified DRG neurons were established by cycling the cultures for 12 d, 2 d each, between NBF medium (Neurobasal [Gibco], B27 supplement [Gibco], 2 mM L-glutamine, 50 ng/ml NGF, penicillin/streptomycin, FUdR [10 µM 5-Fluoro-2′-deoxyuridine {Sigma-Aldrich} + 10 µM uridine {Sigma-Aldrich}]) and NB medium (NBF medium without FUdR) to eliminate fibroblasts and SCs.

Fc fusion binding and clustering experiments

Plasmids encoding IgG Fc fusion proteins were previously described (Kanagawa et al., 2004; Eshed et al., 2005). In brief, for the construction of the α-DG IgG Fc fusion proteins the following α-DG sequences were inserted into the expression construct IgG1FcpcDNA3 (Chen et al., 1996): DGFc2, residues 30–316; DGFc5, residues 30–653; and DGFc6, residues 317–653 (Kunz et al., 2001). Dg-Fc fusion constructs were a gift from K. Campbell. Fc fusions containing either the extracellular domain of gliomedin (ECD-Fc; residues 49–543), its collagen repeats (COL-Fc; residues 49–294), or the olfactomedin domain (Olf-Fc; residues 288–543) were made by cloning the corresponding DNA to pSecTagA vector (Invitrogen), which contains the signal sequence of the κ chain of human IgG, and then transferred to pCX-Fc (Gollan et al., 2003). NrCAM-Fc and Neurofascin-Fc (NF186Fc) contain the entire extracellular domain of the proteins in fusion with human Fc and were produced as described previously (M. Grumet, Rutgers University, Piscataway NJ; Lustig et al., 2001; Koticha et al., 2005). For NF186, the rat cDNA up to nucleotide 4654 was PCR amplified and cloned into the EcoRV site of the pCR3.1/Fc plasmid (Haspel et al., 2000). 293FT cells were transfected with plasmids encoding DG-Fc2, DG-Fc5, DG-Fc6, ECD-Fc, or Olf-Fc in media containing DMEM, 1% Ultra-Low IgG FBS (Invitrogen), and 2 mM L-glutamine. After 72 h, the supernatants were collected and filtered, and Fc protein expression was confirmed by Western blotting. For binding experiments, cells were incubated with conditioned media containing various Fc fusions for 30 min at room temperature. Cells were then washed with PBS, fixed with 4% paraformaldehyde for 5 min at room temperature, and incubated with a Rhodamine-conjugated anti–human Fc antibody (Jackson ImmunoResearch Laboratories, Inc.). Conditioned media containing DG-Fc2 and Olf-Fc were preclustered with the secondary antibody for 30 min before the binding procedure. Clustering experiments were performed as described in Eshed et al. (2005, 2007) with a few modifications. In brief, coverslips were coated with 0.4 mg/ml matrigel (BD) and 100 µg/ml Poly-L-lysine (Sigma-Aldrich). Neurons devoided of SCs after 12 d in vitro were exposed to Fc protein with or without perlecan. Fc proteins containing medium collected from transfected HEK293T cells was incubated for 30 min at room temperature for preclustering with 1 µg/ml Cy3-conjugated goat anti–human antibody (Jackson ImmunoResearch Laboratories, Inc.), with or without 2.25 µg/ml of purified recombinant perlecan. DRG neurons were incubated with preclustered Fc protein medium for 30 min at room temperature, washed once with Neurobasal medium, and incubated with NB medium at 37°C with 5% CO_2 for 3 d. The experiment was repeated at least eight times. After fixation in 4% paraformaldehyde (Sigma-Aldrich) in PBS for 7 min at room temperature (for binding-only control, cells were fixed after incubation with Fc-protein medium), antibody labeling was performed: cells were washed with PBS and incubated in blocking solution (PBS, 5% normal goat serum [Dako], 0.1% Triton X-100, and 1% glycine in the case of binding experiments) for 30 min. Primary antibodies diluted in blocking solution were added for 1 h at room temperature, followed by washing with PBS and incubation with secondary antibodies for 40 min. Coverslips were then washed, mounted in Vectashield (Vector Laboratories), and analyzed on a confocal microscope (UltraView ERS, SP5; Leica) or an Apotome (Carl Zeiss).

Recombinant perlecan

Human recombinant perlecan was produced by transfecting the plasmid pSec-perlecan (gift of K. Sekiguchi, Osaka University, Osaka, Japan), containing full-length human perlecan cDNA (GenBank accession no. NM_005529) in the psectag2B vector; under the control of the cytomegalovirus promoter in HEK293 cells. After zeocin selection, cells were grown as described previously (Bretscher et al., 2002), and their conditioned media was run on a DEAE-sephacel column. The column was washed with 300 mM NaCl (in 50 mM tris, pH 7.4, and 1 mM EDTA) and eluted with 500 mM NaCl (in 50 mM tris, pH 7.4, and 1 mM EDTA). The eluate was diluted to 150 mM NaCl and purified using a colbalt HisPur column (Sigma-Aldrich). This column was washed with 50 mM sodium phosphate buffer, 300 mM NaCl, and 10 mM imidizol. Eluation was obtained with 400 mM imidizol in the same buffer. The resulting protein was dialyzed in TBS buffer (50 mM tris, pH 7.4, with 90 mM NaCl and 0.125 mM EDTA) and then concentrated using an Amicon Ultra 100K MWCO filter (EMD Millipore).

Far Western analysis

Fc-tagged proteins were purified from the medium by adding 0.150 ml of protein A Sepharose beads (IPA-400HC; Repligen) per 50-ml tube. The tubes were placed on a rotating wheel at 4°C overnight, and then spun at 1,000 rpm (206 *g*) for 5 min. Next, the supernatant was decanted and beads were resuspended in the remaining liquid and transferred to a chromatography mini-column (Bio-Rad Laboratories). After washing in PBS, the proteins were eluted with 4 bed-volumes of 0.1 M glycine, pH 2.6, and neutralized immediately with 1 M Tris, pH 9.0. The Fc-tagged proteins were dialyzed in TBS buffer (50 mM tris, pH 7.4, with 90 mM NaCl and 0.125 mM EDTA) and quantified using a BCA kit (Invitrogen). Recombinant perlecan or BSA were spotted on dry nitrocellulose; blocked with 50 mM Tris-HCl, pH 7.5, 150 mM NaCl, 0.1% Tween-20, and 10% milk; washed; and incubated with purified Fc fusion prey proteins. After washing, the bound Fc proteins were detected using protein G–HRP.

ELISA analysis

Wells were coated with 0.5 µg/ml of recombinant perlecan, and purified Fc fusion proteins were added for 2 h, washed, treated with anti–human Fc-HRP for 1 h, and revealed for 5 min with TMB ELISA Substrate (Thermo Fisher Scientific).

Heparinase treatment and solid-phase perlecan binding assay

Perlecan was coated onto the wells of high-binding Costar dishes at 5 µg/ml in 0.15 M sodium bicarbonate overnight at 4°C. An aliquot (7.5 µg in 35 µl) of perlecan was treated with heparinase (Seikigaku-Kogyo/Amsbio) at 37°C for 20 h with 25 mU before coating. Dishes were blocked for 1 h at room temperature with 3% BSA in 50 mM Tris, pH 7.4, 90 mM NaCl,

Published February 2, 2015

and 1 mM $CaCl_2$. Gliomedin-Fc protein was added to the perlecan-coated dishes at the indicated concentrations in blocking buffer and incubated for 1 h at room temperature. After washing off unbound protein, the bound species was detected with 1:5,000 anti–Fc-HRP (Thermo Fisher Scientific) and Ultra TMB substrate (Thermo Fisher Scientific). Absorbance was determined at 450 nM with a Spectra Fluor multichannel plate reader.

Image acquisition, processing, and quantification

Immunofluorescence stainings of teased fibers and cultures were imaged at room temperature using one of the following four microscopes. UltraView ERS spinning disk confocal microscope (PerkinElmer) with the Volocity acquisition software, adapted with a Plan Apochromat 63× (NA 1.4) Oil objective and a camera (C9100-02; Hamamatsu Photonics). TCS-SP2 or SP5II confocal fluorescence microscope (Leica) equipped with a Plan Apochromat 63 Å/1.4 or HCX PLAPO 100×/1.44 oil CORR CS oil-immersion objectives and using the LCS confocal acquisition software (LAS AF Version 2.6.3.8173; Leica). Observer (Carl Zeiss) equipped with Apotome.2 and Axiovision software v. 4.8.2.0, a 40×/1.30 M27EC Plan-Neofluar oil objective and a high resolution microscopy camera (AxioCam MRm Rev. 3 FireWire). FITC, TRITC, and cy-5 fluorophores were excited with an Ar laser (488 nm), a He/Ne laser (568 nm), and a red diode laser (640 nm), respectively.

Figures were assembled using Photoshop software (Adobe). None or minimal modification to the images was performed with Photoshop; all the images in each panel were treated identically at every step. To quantify the frequency of abnormal Nav clusters, images were photographed using TCS-SP2 or SP5 confocal fluorescence microscopes (Leica) equipped with a Plan Apochromat 63 Å/1.4 oil-immersion objective and using the LCS confocal acquisition software (Leica). The gain of Nav fluorescence detection was maintained below the threshold of fluorochrome saturation. z-axis series spanning ∼3.0 µm were acquired as 1,024 × 1,024-pixel images by sequentially scanning (between frames), using a step size of 0.1221 µm. To quantify nodal clusters on DRG cultures, four to five z-images per field were acquired in identical conditions with an Apotome microscope (Carl Zeiss), favoring areas that contained good clusters and did not contain axonal initial segments. Fiji software was then used to generate maximum projections, split colors, adjust thresholds, and display only red (Fc-gliomedin) and green (βIV spectrin) colocalized particles. Fiji was then used to count and measure these particles. Particles were checked visually to eliminate clusters that were not on axons, that were on axonal initial segments, or that were part or nonspecific precipitates.

Online supplemental material

Fig. S1 shows the expression of laminin α5 during nerve and node development. Fig. S2 shows that pharmacological inhibition of furin impairs myelination and nodogenesis in DRG co-cultures. Fig. S3 shows the expression of perlecan, β-DG, versican 1, syndecan 3, and agrin in perlecan mutant nerves. Fig. S4 shows the binding affinity of gliomedin to perlecan with or without heparinase treatment and in comparison to α-DG. Online supplemental material is available at http://www.jcb.org/cgi/content/full/jcb.201403111/DC1.

We thank C. Williamson for superb technical assistance; Y. Poitelon for artwork; the Advanced Light and Electron Microscopy Bioimaging Center at San Raffaele for imaging; K. Campbell for *Dag*-floxed mice, Fc-DG constructs, and antibodies; K. Sekiguchi for perlecan plasmid; M. Rasband for Fc constructs and antibodies; M. Grumet for Fc constructs; and F. Saito, M. Dours Zimmermann, L. Sorokin, J. Trimmer, M. Ruegg, V. Lee, and P. Brophy for antibodies.

This work was supported by R01 NS045630 (to M.L. Feltri), NS055256 (to L. Wrabetz), NS50220 (to E. Peles), and DK36425 (to P. Yurchenco); the Dr. Miriam and Sheldon G. Adelson Medical Research Foundation; the Israel Science Foundation; and the European Community's Seventh Framework Program UE-FP7 (Neuron–Glia Interactions in Nerve Development and Disease).

The authors declare no competing financial interests.

Submitted: 26 March 2014
Accepted: 18 December 2014

References

Apostolski, S., S.A. Sadiq, A. Hays, M. Corbo, L. Suturkova-Milosevic, P. Chaliff, K. Stefansson, R.G. LeBaron, E. Ruoslahti, A.P. Hays, et al. 1994. Identification of Gal(β1–3)GalNAc bearing glycoproteins at the nodes of Ranvier in peripheral nerve. *J. Neurosci. Res.* 38:134–141. http://dx.doi.org/10.1002/jnr.490380203

Arikawa-Hirasawa, E., H. Watanabe, H. Takami, J.R. Hassell, and Y. Yamada. 1999. Perlecan is essential for cartilage and cephalic development. *Nat. Genet.* 23:354–358. http://dx.doi.org/10.1038/15537

Bangratz, M., N. Sarrazin, J. Devaux, D. Zambroni, A. Echaniz-Laguna, F. René, D. Boërio, C.S. Davoine, B. Fontaine, M.L. Feltri, et al. 2012. A mouse model of Schwartz-Jampel syndrome reveals myelinating Schwann cell dysfunction with persistent axonal depolarization in vitro and distal peripheral nerve hyperexcitability when perlecan is lacking. *Am. J. Pathol.* 180:2040–2055. http://dx.doi.org/10.1016/j.ajpath.2012.01.035

Bekku, Y., L. Vargová, Y. Goto, I. Vorísek, L. Dmytrenko, M. Narasaki, A. Ohtsuka, R. Fässler, Y. Ninomiya, E. Syková, and T. Oohashi. 2010. Bral1: its role in diffusion barrier formation and conduction velocity in the CNS. *J. Neurosci.* 30:3113–3123. http://dx.doi.org/10.1523/JNEUROSCI.5598-09.2010

Bhat, M.A., J.C. Rios, Y. Lu, G.P. Garcia-Fresco, W. Ching, M. St Martin, J. Li, S. Einheber, M. Chesler, J. Rosenbluth, et al. 2001. Axon-glia interactions and the domain organization of myelinated axons requires neurexin IV/Caspr/Paranodin. *Neuron*. 30:369–383. http://dx.doi.org/10.1016/S0896-6273(01)00294-X

Bishop, J.R., M. Schuksz, and J.D. Esko. 2007. Heparan sulphate proteoglycans fine-tune mammalian physiology. *Nature*. 446:1030–1037. http://dx.doi.org/10.1038/nature05817

Bix, G., and R.V. Iozzo. 2008. Novel interactions of perlecan: unraveling perlecan's role in angiogenesis. *Microsc. Res. Tech.* 71:339–348. http://dx.doi.org/10.1002/jemt.20562

Boiko, T., M.N. Rasband, S.R. Levinson, J.H. Caldwell, G. Mandel, J.S. Trimmer, and G. Matthews. 2001. Compact myelin dictates the differential targeting of two sodium channel isoforms in the same axon. *Neuron*. 30:91–104. http://dx.doi.org/10.1016/S0896-6273(01)00265-3

Brakebusch, C., C.I. Seidenbecher, F. Asztely, U. Rauch, H. Matthies, H. Meyer, M. Krug, T.M. Böckers, X. Zhou, M.R. Kreutz, et al. 2002. Brevican-deficient mice display impaired hippocampal CA1 long-term potentiation but show no obvious deficits in learning and memory. *Mol. Cell. Biol.* 22:7417–7427. http://dx.doi.org/10.1128/MCB.22.21.7417-7427.2002

Bretscher, A., K. Edwards, and R.G. Fehon. 2002. ERM proteins and merlin: integrators at the cell cortex. *Nat. Rev. Mol. Cell Biol.* 3:586–599. http://dx.doi.org/10.1038/nrm882

Cai, H., R.A. Erdman, L. Zweier, J. Chen, J.H. Shaw IV, K.A. Baylor, M.M. Stecker, D.J. Carey, and Y.M. Chan. 2007. The sarcoglycan complex in Schwann cells and its role in myelin stability. *Exp. Neurol.* 205:257–269. http://dx.doi.org/10.1016/j.expneurol.2007.02.015

Chen, Y., T. Maguire, and R.M. Marks. 1996. Demonstration of binding of dengue virus envelope protein to target cells. *J. Virol.* 70:8765–8772.

Court, F.A., D.L. Sherman, T. Pratt, E.M. Garry, R.R. Ribchester, D.F. Cottrell, S.M. Fleetwood-Walker, and P.J. Brophy. 2004. Restricted growth of Schwann cells lacking Cajal bands slows conduction in myelinated nerves. *Nature*. 431:191–195. http://dx.doi.org/10.1038/nature02841

Court, F.A., J.E. Hewitt, K. Davies, B.L. Patton, A. Uncini, L. Wrabetz, and M.L. Feltri. 2009. A laminin-2, dystroglycan, utrophin axis is required for compartmentalization and elongation of myelin segments. *J. Neurosci.* 29:3908–3919. http://dx.doi.org/10.1523/JNEUROSCI.5672-08.2009

Court, F.A., D. Zambroni, E. Pavoni, C. Colombelli, C. Baragli, G. Figlia, L. Sorokin, W. Ching, J.L. Salzer, L. Wrabetz, and M.L. Feltri. 2011. MMP2-9 cleavage of dystroglycan alters the size and molecular composition of Schwann cell domains. *J. Neurosci.* 31:12208–12217. http://dx.doi.org/10.1523/JNEUROSCI.0141-11.2011

Custer, A.W., K. Kazarinova-Noyes, T. Sakurai, X. Xu, W. Simon, M. Grumet, and P. Shrager. 2003. The role of the ankyrin-binding protein NrCAM in node of Ranvier formation. *J. Neurosci.* 23:10032–10039.

Dours-Zimmermann, M.T., K. Maurer, U. Rauch, W. Stoffel, R. Fässler, and D.R. Zimmermann. 2009. Versican V2 assembles the extracellular matrix surrounding the nodes of ranvier in the CNS. *J. Neurosci.* 29:7731–7742. http://dx.doi.org/10.1523/JNEUROSCI.4158-08.2009

Dzhashiashvili, Y., Y. Zhang, J. Galinska, I. Lam, M. Grumet, and J.L. Salzer. 2007. Nodes of Ranvier and axon initial segments are ankyrin G–dependent domains that assemble by distinct mechanisms. *J. Cell Biol.* 177:857–870. http://dx.doi.org/10.1083/jcb.200612012

Elfvin, L.G. 1961. The ultrastructure of the nodes of Ranvier in cat sympathetic nerve fibers. *J. Ultrastruct. Res.* 5:374–387. http://dx.doi.org/10.1016/S0022-5320(61)80014-2

Eshed, Y., K. Feinberg, S. Poliak, H. Sabanay, O. Sarig-Nadir, I. Spiegel, J.R. Bermingham Jr., and E. Peles. 2005. Gliomedin mediates Schwann cell-axon interaction and the molecular assembly of the nodes of Ranvier. *Neuron*. 47:215–229. http://dx.doi.org/10.1016/j.neuron.2005.06.026

Published February 2, 2015

Eshed, Y., K. Feinberg, D.J. Carey, and E. Peles. 2007. Secreted gliomedin is a perinodal matrix component of peripheral nerves. *J. Cell Biol.* 177:551–562. http://dx.doi.org/10.1083/jcb.200612139

Eshed-Eisenbach, Y., and E. Peles. 2013. The making of a node: a co-production of neurons and glia. *Curr. Opin. Neurobiol.* 23:1049–1056. http://dx.doi.org/10.1016/j.conb.2013.06.003

Farach-Carson, M.C., C.R. Warren, D.A. Harrington, and D.D. Carson. 2014. Border patrol: Insights into the unique role of perlecan/heparan sulfate proteoglycan 2 at cell and tissue borders. *Matrix Biol.* 34:64–79.

Feinberg, K., Y. Eshed-Eisenbach, S. Frechter, V. Amor, D. Salomon, H. Sabanay, J.L. Dupree, M. Grumet, P.J. Brophy, P. Shrager, and E. Peles. 2010. A glial signal consisting of gliomedin and NrCAM clusters axonal Na^+ channels during the formation of nodes of Ranvier. *Neuron*. 65:490–502. http://dx.doi.org/10.1016/j.neuron.2010.02.004

Feltri, M.L., S.S. Scherer, L. Wrabetz, J. Kamholz, and M.E. Shy. 1992. Mitogen-expanded Schwann cells retain the capacity to myelinate regenerating axons after transplantation into rat sciatic nerve. *Proc. Natl. Acad. Sci. USA*. 89:8827–8831. http://dx.doi.org/10.1073/pnas.89.18.8827

Feltri, M.L., S.S. Scherer, R. Nemni, J. Kamholz, H. Vogelbacker, M.O. Scott, N. Canal, V. Quaranta, and L. Wrabetz. 1994. β4 integrin expression in myelinating Schwann cells is polarized, developmentally regulated and axonally dependent. *Development*. 120:1287–1301.

Feltri, M.L., M. D'Antonio, S. Previtali, M. Fasolini, A. Messing, and L. Wrabetz. 1999. P_0-*Cre* transgenic mice for inactivation of adhesion molecules in Schwann cells. *Ann. NY Acad. Sci.* 883:116–123. http://dx.doi.org/10.1111/j.1749-6632.1999.tb08574.x

Gesemann, M., A. Brancaccio, B. Schumacher, and M.A. Ruegg. 1998. Agrin is a high-affinity binding protein of dystroglycan in non-muscle tissue. *J. Biol. Chem.* 273:600–605. http://dx.doi.org/10.1074/jbc.273.1.600

Gollan, L., D. Salomon, J.L. Salzer, and E. Peles. 2003. Caspr regulates the processing of contactin and inhibits its binding to neurofascin. *J. Cell Biol.* 163:1213–1218. http://dx.doi.org/10.1083/jcb.200309147

Goutebroze, L., M. Carnaud, N. Denisenko, M.C. Boutterin, and J.A. Girault. 2003. Syndecan-3 and syndecan-4 are enriched in Schwann cell perinodal processes. *BMC Neurosci.* 4:29. http://dx.doi.org/10.1186/1471-2202-4-29

Handler, M., P.D. Yurchenco, and R.V. Iozzo. 1997. Developmental expression of perlecan during murine embryogenesis. *Dev. Dyn.* 210:130–145. http://dx.doi.org/10.1002/(SICI)1097-0177(199710)210:2<130::AID-AJA6>3.0.CO;2-H

Haspel, J., D.R. Friedlander, N. Ivgy-May, S. Chickramane, C. Roonprapunt, S. Chen, M. Schachner, and M. Grumet. 2000. Critical and optimal Ig domains for promotion of neurite outgrowth by L1/Ng-CAM. *J. Neurobiol.* 42:287–302. http://dx.doi.org/10.1002/(SICI)1097-4695(20000215)42:3<287::AID-NEU1>3.0.CO;2-X

Hedstrom, K.L., X. Xu, Y. Ogawa, R. Frischknecht, C.I. Seidenbecher, P. Shrager, and M.N. Rasband. 2007. Neurofascin assembles a specialized extracellular matrix at the axon initial segment. *J. Cell Biol.* 178:875–886. http://dx.doi.org/10.1083/jcb.200705119

Hess, A., and J.Z. Young. 1952. The nodes of Ranvier. *Proc. R. Soc. Lond. B Biol. Sci.* 140:301–320. http://dx.doi.org/10.1098/rspb.1952.0063

Hildebrand, C. 1971. Ultrastructural and light-microscopic studies of the developing feline spinal cord white matter. I. The nodes of Ranvier. *Acta Physiol. Scand. Suppl.* 82:81–107. http://dx.doi.org/10.1111/j.1365-201X.1971.tb10979.x

Hildebrand, C., and S.G. Waxman. 1984. Postnatal differentiation of rat optic nerve fibers: electron microscopic observations on the development of nodes of Ranvier and axoglial relations. *J. Comp. Neurol.* 224:25–37. http://dx.doi.org/10.1002/cne.902240103

Hnia, K., G. Hugon, A. Masmoudi, J. Mercier, F. Rivier, and D. Mornet. 2006. Effect of β-dystroglycan processing on utrophin/Dp116 anchorage in normal and mdx mouse Schwann cell membrane. *Neuroscience*. 141:607–620. http://dx.doi.org/10.1016/j.neuroscience.2006.04.043

Hodgkin, A.L., and A.F. Huxley. 1952. A quantitative description of membrane current and its application to conduction and excitation in nerve. *J. Physiol.* 117:500–544. http://dx.doi.org/10.1113/jphysiol.1952.sp004764

Ichimura, T., and M.H. Ellisman. 1991. Three-dimensional fine structure of cytoskeletal-membrane interactions at nodes of Ranvier. *J. Neurocytol.* 20:667–681. http://dx.doi.org/10.1007/BF01187068

Kanagawa, M., F. Saito, S. Kunz, T. Yoshida-Moriguchi, R. Barresi, Y.M. Kobayashi, J. Muschler, J.P. Dumanski, D.E. Michele, M.B. Oldstone, and K.P. Campbell. 2004. Molecular recognition by LARGE is essential for expression of functional dystroglycan. *Cell*. 117:953–964. http://dx.doi.org/10.1016/j.cell.2004.06.003

Kaplan, M.R., A. Meyer-Franke, S. Lambert, V. Bennett, I.D. Duncan, S.R. Levinson, and B.A. Barres. 1997. Induction of sodium channel clustering by oligodendrocytes. *Nature*. 386:724–728. http://dx.doi.org/10.1038/386724a0

Kaplan, M.R., M.H. Cho, E.M. Ullian, L.L. Isom, S.R. Levinson, and B.A. Barres. 2001. Differential control of clustering of the sodium channels $Na_v1.2$ and $Na_v1.6$ at developing CNS nodes of Ranvier. *Neuron*. 30:105–119. http://dx.doi.org/10.1016/S0896-6273(01)00266-5

Komada, M., and P. Soriano. 2002. βIV-spectrin regulates sodium channel clustering through ankyrin-G at axon initial segments and nodes of Ranvier. *J. Cell Biol.* 156:337–348. http://dx.doi.org/10.1083/jcb.200110003

Koticha, D., J. Babiarz, N. Kane-Goldsmith, J. Jacob, K. Raju, and M. Grumet. 2005. Cell adhesion and neurite outgrowth are promoted by neurofascin NF155 and inhibited by NF186. *Mol. Cell. Neurosci.* 30:137–148. http://dx.doi.org/10.1016/j.mcn.2005.06.007

Koticha, D., P. Maurel, G. Zanazzi, N. Kane-Goldsmith, S. Basak, J. Babiarz, J. Salzer, and M. Grumet. 2006. Neurofascin interactions play a critical role in clustering sodium channels, $ankyrin_G$ and βIV spectrin at peripheral nodes of Ranvier. *Dev. Biol.* 293:1–12. http://dx.doi.org/10.1016/j.ydbio.2005.05.028

Kunz, S., N. Sevilla, D.B. McGavern, K.P. Campbell, and M.B. Oldstone. 2001. Molecular analysis of the interaction of LCMV with its cellular receptor α-dystroglycan. *J. Cell Biol.* 155:301–310. http://dx.doi.org/10.1083/jcb.200104103

Kwok, J.C., G. Dick, D. Wang, and J.W. Fawcett. 2011. Extracellular matrix and perineuronal nets in CNS repair. *Dev. Neurobiol.* 71:1073–1089. http://dx.doi.org/10.1002/dneu.20974

Labasque, M., J.J. Devaux, C. Lévêque, and C. Faivre-Sarrailh. 2011. Fibronectin type III-like domains of neurofascin-186 protein mediate gliomedin binding and its clustering at the developing nodes of Ranvier. *J. Biol. Chem.* 286:42426–42434. http://dx.doi.org/10.1074/jbc.M111.266353

Lacas-Gervais, S., J. Guo, N. Strenzke, E. Scarfone, M. Kolpe, M. Jahkel, P. De Camilli, T. Moser, M.N. Rasband, and M. Solimena. 2004. βIVΣ1 spectrin stabilizes the nodes of Ranvier and axon initial segments. *J. Cell Biol.* 166:983–990. http://dx.doi.org/10.1083/jcb.200408007

Lambert, S., J.Q. Davis, and V. Bennett. 1997. Morphogenesis of the node of Ranvier: co-clusters of ankyrin and ankyrin-binding integral proteins define early developmental intermediates. *J. Neurosci.* 17:7025–7036.

Landon, D.N., and O.K. Langley. 1971. The local chemical environment of nodes of Ranvier: a study of cation binding. *J. Anat.* 108:419–432.

Lustig, M., L. Erskine, C.A. Mason, M. Grumet, and T. Sakurai. 2001. Nr-CAM expression in the developing mouse nervous system: ventral midline structures, specific fiber tracts, and neuropilar regions. *J. Comp. Neurol.* 434:13–28. http://dx.doi.org/10.1002/cne.1161

Maertens, B., D. Hopkins, C.W. Franzke, D.R. Keene, L. Bruckner-Tuderman, D.S. Greenspan, and M. Koch. 2007. Cleavage and oligomerization of gliomedin, a transmembrane collagen required for node of Ranvier formation. *J. Biol. Chem.* 282:10647–10659. http://dx.doi.org/10.1074/jbc.M611339200

Martin, P.T. 2003. Dystroglycan glycosylation and its role in matrix binding in skeletal muscle. *Glycobiology*. 13:55R–66R. http://dx.doi.org/10.1093/glycob/cwg076

Martin, S., A.K. Levine, Z.J. Chen, Y. Ughrin, and J.M. Levine. 2001. Deposition of the NG2 proteoglycan at nodes of Ranvier in the peripheral nervous system. *J. Neurosci.* 21:8119–8128.

Melendez-Vasquez, C., D.J. Carey, G. Zanazzi, O. Reizes, P. Maurel, and J.L. Salzer. 2005. Differential expression of proteoglycans at central and peripheral nodes of Ranvier. *Glia*. 52:301–308. http://dx.doi.org/10.1002/glia.20245

Moore, S.A., F. Saito, J. Chen, D.E. Michele, M.D. Henry, A. Messing, R.D. Cohn, S.E. Ross-Barta, S. Westra, R.A. Williamson, et al. 2002. Deletion of brain dystroglycan recapitulates aspects of congenital muscular dystrophy. *Nature*. 418:422–425. http://dx.doi.org/10.1038/nature00838

Nico, B., R. Tamma, T. Annese, D. Mangieri, A. De Luca, P. Corsi, V. Benagiano, V. Longo, E. Crivellato, A. Salmaggi, and D. Ribatti. 2010. Glial dystrophin-associated proteins, laminin and agrin, are downregulated in the brain of mdx mouse. *Lab. Invest.* 90:1645–1660. http://dx.doi.org/10.1038/labinvest.2010.149

Occhi, S., D. Zambroni, U. Del Carro, S. Amadio, E.E. Sirkowski, S.S. Scherer, K.P. Campbell, S.A. Moore, Z.L. Chen, S. Strickland, et al. 2005. Both laminin and Schwann cell dystroglycan are necessary for proper clustering of sodium channels at nodes of Ranvier. *J. Neurosci.* 25:9418–9427. http://dx.doi.org/10.1523/JNEUROSCI.2068-05.2005

Pan, Z., T. Kao, Z. Horvath, J. Lemos, J.Y. Sul, S.D. Cranstoun, V. Bennett, S.S. Scherer, and E.C. Cooper. 2006. A common ankyrin-G-based mechanism retains KCNQ and Na_V channels at electrically active domains of the axon. *J. Neurosci.* 26:2599–2613. http://dx.doi.org/10.1523/JNEUROSCI.4314-05.2006

Pedraza, L., J.K. Huang, and D.R. Colman. 2001. Organizing principles of the axoglial apparatus. *Neuron*. 30:335–344. http://dx.doi.org/10.1016/S0896-6273(01)00306-3

Peters, A. 1966. The node of Ranvier in the central nervous system. *Q. J. Exp. Physiol. Cogn. Med. Sci.* 51:229–236.

Raine, C.S. 1984. On the association between perinodal astrocytic processes and the node of Ranvier in the C.N.S. *J. Neurocytol.* 13:21–27. http://dx.doi.org/10.1007/BF01148316

Ranvier, L. 1871. Sur les éléments conjonctifs de la moelle épinière. *Comptes Rendus de l'Académie des Sciences*. 73:1168–1171.

Rieger, F., J.K. Daniloff, M. Pincon-Raymond, K.L. Crossin, M. Grumet, and G.M. Edelman. 1986. Neuronal cell adhesion molecules and cytotactin are colocalized at the node of Ranvier. *J. Cell Biol.* 103:379–391. http://dx.doi.org/10.1083/jcb.103.2.379

Rossi, M., H. Morita, R. Sormunen, S. Airenne, M. Kreivi, L. Wang, N. Fukai, B.R. Olsen, K. Tryggvason, and R. Soininen. 2003. Heparan sulfate chains of perlecan are indispensable in the lens capsule but not in the kidney. *EMBO J.* 22:236–245. http://dx.doi.org/10.1093/emboj/cdg019

Saito, F., S.A. Moore, R. Barresi, M.D. Henry, A. Messing, S.E. Ross-Barta, R.D. Cohn, R.A. Williamson, K.A. Sluka, D.L. Sherman, et al. 2003. Unique role of dystroglycan in peripheral nerve myelination, nodal structure, and sodium channel stabilization. *Neuron*. 38:747–758. http://dx.doi.org/10.1016/S0896-6273(03)00301-5

Saito, F., Y. Saito-Arai, A. Nakamura, T. Shimizu, and K. Matsumura. 2008. Processing and secretion of the N-terminal domain of α-dystroglycan in cell culture media. *FEBS Lett.* 582:439–444. http://dx.doi.org/10.1016/j.febslet.2008.01.006

Schafer, D.P., A.W. Custer, P. Shrager, and M.N. Rasband. 2006. Early events in node of Ranvier formation during myelination and remyelination in the PNS. *Neuron Glia Biol.* 2:69–79. http://dx.doi.org/10.1017/S1740925X06000093

Sherman, D.L., S. Tait, S. Melrose, R. Johnson, B. Zonta, F.A. Court, W.B. Macklin, S. Meek, A.J. Smith, D.F. Cottrell, and P.J. Brophy. 2005. Neurofascins are required to establish axonal domains for saltatory conduction. *Neuron*. 48:737–742. http://dx.doi.org/10.1016/j.neuron.2005.10.019

Singh, J., Y. Itahana, S. Knight-Krajewski, M. Kanagawa, K.P. Campbell, M.J. Bissell, and J. Muschler. 2004. Proteolytic enzymes and altered glycosylation modulate dystroglycan function in carcinoma cells. *Cancer Res.* 64:6152–6159. http://dx.doi.org/10.1158/0008-5472.CAN-04-1638

Skarnes, W.C., J.E. Moss, S.M. Hurtley, and R.S. Beddington. 1995. Capturing genes encoding membrane and secreted proteins important for mouse development. *Proc. Natl. Acad. Sci. USA*. 92:6592–6596. http://dx.doi.org/10.1073/pnas.92.14.6592

Spence, H.J., Y.J. Chen, C.L. Batchelor, J.R. Higginson, H. Suila, O. Carpen, and S.J. Winder. 2004. Ezrin-dependent regulation of the actin cytoskeleton by β-dystroglycan. *Hum. Mol. Genet.* 13:1657–1668. http://dx.doi.org/10.1093/hmg/ddh170

Stum, M., E. Girard, M. Bangratz, V. Bernard, M. Herbin, A. Vignaud, A. Ferry, C.S. Davoine, A. Echaniz-Laguna, F. René, et al. 2008. Evidence of a dosage effect and a physiological endplate acetylcholinesterase deficiency in the first mouse models mimicking Schwartz-Jampel syndrome neuromyotonia. *Hum. Mol. Genet.* 17:3166–3179. http://dx.doi.org/10.1093/hmg/ddn213

Susuki, K., K.J. Chang, D.R. Zollinger, Y. Liu, Y. Ogawa, Y. Eshed-Eisenbach, M.T. Dours-Zimmermann, J.A. Oses-Prieto, A.L. Burlingame, C.I. Seidenbecher, et al. 2013. Three mechanisms assemble central nervous system nodes of Ranvier. *Neuron*. 78:469–482. http://dx.doi.org/10.1016/j.neuron.2013.03.005

Talts, J.F., Z. Andac, W. Göhring, A. Brancaccio, and R. Timpl. 1999. Binding of the G domains of laminin α1 and α2 chains and perlecan to heparin, sulfatides, α-dystroglycan and several extracellular matrix proteins. *EMBO J.* 18:863–870. http://dx.doi.org/10.1093/emboj/18.4.863

Tao-Cheng, J.H., and J. Rosenbluth. 1983. Axolemmal differentiation in myelinated fibers of rat peripheral nerves. *Brain Res.* 9:251–263. http://dx.doi.org/10.1016/0165-3806(83)90023-8

Thaxton, C., A.M. Pillai, A.L. Pribisko, J.L. Dupree, and M.A. Bhat. 2011. Nodes of Ranvier act as barriers to restrict invasion of flanking paranodal domains in myelinated axons. *Neuron*. 69:244–257. http://dx.doi.org/10.1016/j.neuron.2010.12.016

Voas, M.G., D.A. Lyons, S.G. Naylor, N. Arana, M.N. Rasband, and W.S. Talbot. 2007. αII-spectrin is essential for assembly of the nodes of Ranvier in myelinated axons. *Curr. Biol.* 17:562–568. http://dx.doi.org/10.1016/j.cub.2007.01.071

Walko, G., K.L. Wögenstein, L. Winter, I. Fischer, M.L. Feltri, and G. Wiche. 2013. Stabilization of the dystroglycan complex in Cajal bands of myelinating Schwann cells through plectin-mediated anchorage to vimentin filaments. *Glia*. 61:1274–1287. http://dx.doi.org/10.1002/glia.22514

Waxman, S.G., and J.A. Black. 1984. Freeze-fracture ultrastructure of the perinodal astrocyte and associated glial junctions. *Brain Res.* 308:77–87. http://dx.doi.org/10.1016/0006-8993(84)90919-3

Weber, P., U. Bartsch, M.N. Rasband, R. Czaniera, Y. Lang, H. Bluethmann, R.U. Margolis, S.R. Levinson, P. Shrager, D. Montag, and M. Schachner. 1999. Mice deficient for tenascin-R display alterations of the extracellular matrix and decreased axonal conduction velocities in the CNS. *J. Neurosci.* 19:4245–4262.

Whitelock, J.M., J. Melrose, and R.V. Iozzo. 2008. Diverse cell signaling events modulated by perlecan. *Biochemistry*. 47:11174–11183. http://dx.doi.org/10.1021/bi8013938

Winkler, S., R.C. Stahl, D.J. Carey, and R. Bansal. 2002. Syndecan-3 and perlecan are differentially expressed by progenitors and mature oligodendrocytes and accumulate in the extracellular matrix. *J. Neurosci. Res.* 69:477–487. http://dx.doi.org/10.1002/jnr.10311

Yamada, H., F. Saito, H. Fukuta-Ohi, D. Zhong, A. Hase, K. Arai, A. Okuyama, R. Maekawa, T. Shimizu, and K. Matsumura. 2001. Processing of β-dystroglycan by matrix metalloproteinase disrupts the link between the extracellular matrix and cell membrane via the dystroglycan complex. *Hum. Mol. Genet.* 10:1563–1569. http://dx.doi.org/10.1093/hmg/10.15.1563

Yang, Y., S. Lacas-Gervais, D.K. Morest, M. Solimena, and M.N. Rasband. 2004. βIV spectrins are essential for membrane stability and the molecular organization of nodes of Ranvier. *J. Neurosci.* 24:7230–7240. http://dx.doi.org/10.1523/JNEUROSCI.2125-04.2004

Zhang, Y., Y. Bekku, Y. Dzhashiashvili, S. Armenti, X. Meng, Y. Sasaki, J. Milbrandt, and J.L. Salzer. 2012. Assembly and maintenance of nodes of Ranvier rely on distinct sources of proteins and targeting mechanisms. *Neuron*. 73:92–107. http://dx.doi.org/10.1016/j.neuron.2011.10.016

Zhong, D., F. Saito, Y. Saito, A. Nakamura, T. Shimizu, and K. Matsumura. 2006. Characterization of the protease activity that cleaves the extracellular domain of β-dystroglycan. *Biochem. Biophys. Res. Commun.* 345:867–871. http://dx.doi.org/10.1016/j.bbrc.2006.05.004

Zonta, B., S. Tait, S. Melrose, H. Anderson, S. Harroch, J. Higginson, D.L. Sherman, and P.J. Brophy. 2008. Glial and neuronal isoforms of Neurofascin have distinct roles in the assembly of nodes of Ranvier in the central nervous system. *J. Cell Biol.* 181:1169–1177. http://dx.doi.org/10.1083/jcb.200712154

Colombelli et al., http://www.jcb.org/cgi/content/full/jcb.201403111/DC1

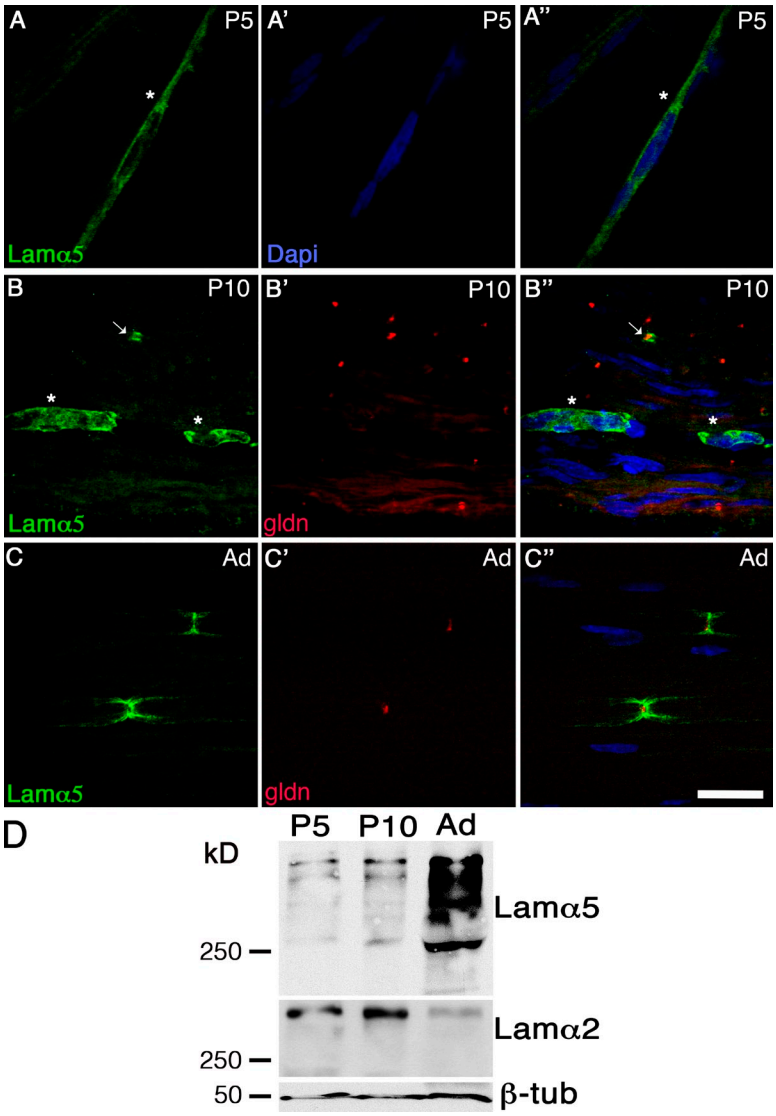

Figure S1. **Laminin 511 accumulates to nodes after they are formed.** Teased fibers from sciatic nerves of P5, P10, and adult (Ad) rats stained for laminin α5 (green; A–C), gliomedin (red; B′–C′), and DAPI (blue) show that at P5 SCs contain perinuclear laminin α5 (asterisk), which accumulates to nodes after P10 (arrow). Bar, 17.5 µm. (D) Western blot of sciatic nerve lysates for laminin α5 confirms late expression of laminin 511. Multiple α5-laminin bands at the expected size of 450, 380, 320, and 210 kD are detected (Miner et al., 1997). For comparison, the same blot was incubated with anti–laminin α2 chain antibody.

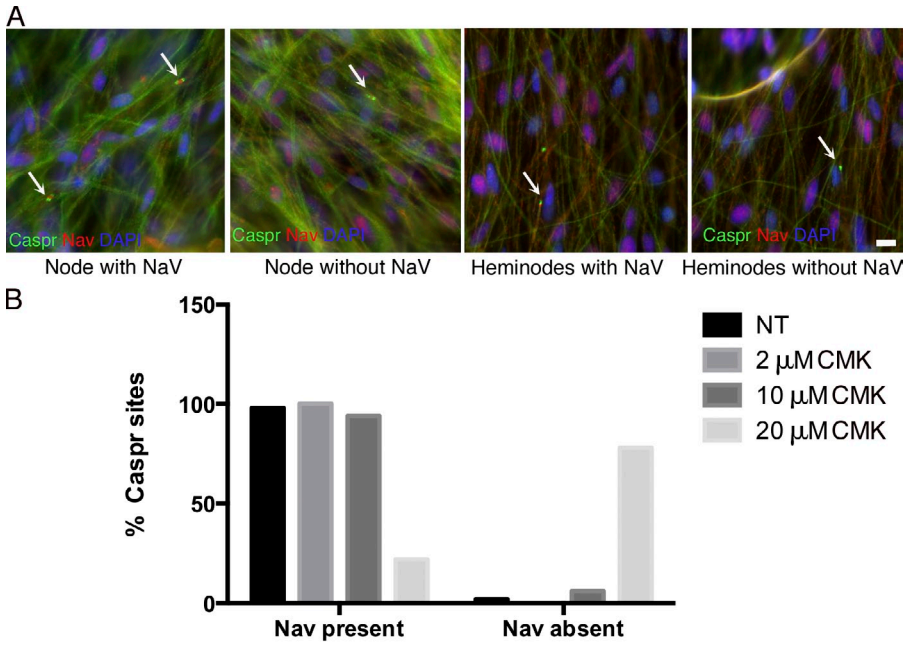

Figure S2. **Furin inhibition reduces clustering of Nav channels in vitro.** (A) Myelinating DRG-SC co-coltures were treated with CMK and stained for Caspr (green), Nav (red), and DAPI (blue). Nodes and heminodes are indicated with arrows. (B) The percentage of paranodes (marked with Caspr) flanked by Nav channels was quantified. 20 μM CMK reduced myelination (not depicted) and the percentage of paranodes flanked by Nav channels ($P < 0.0001$ by χ^2 test). Data from a representative experiment out of two repeats. For the experiment shown, $n = 333$ nodes. Bar, 10 μm.

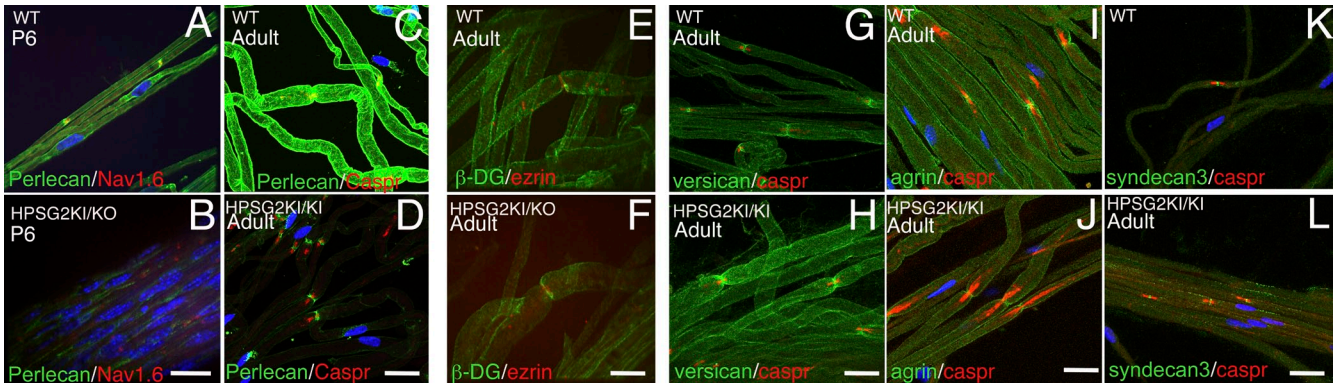

Figure S3. **The expression of other proteoglycans is mantained in perlecan mutants.** Teased fibers from P6 (A and B) or adult (C–L) sciatic nerves from wild-type (A, C, E, G, I, and K), *Hspg2*$^{KI/KO}$ (B and D), or *Hspg2*$^{KI/KI}$ (F, H, J, and L) mice. Staining for perlecan or the indicated proteoglycans at nodes (green), counterstained with nodal and paranodal markers (red), shows that perlecan is absent at nodes in *Hspg2*$^{KI/KO}$ mutants (B) and decreased in *Hspg2*$^{KI/KI}$ mutants (D). The green signal in C and D was increased to show residual perlecan in D. Other proteoglycans at nodes are maintained in *Hspg2* mutants. Fibers are counterstained with DAPI (blue). Bars, 25 μm.

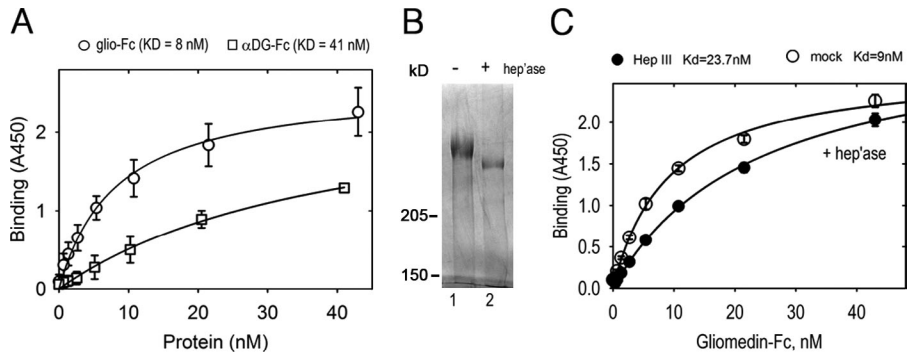

Figure S4. **Gliomedin binds with high affinity to perlecan HS chain and core protein.** (A) Binding of gliomedin-Fc or DG-Fc5 to perlecan by solid-phase assay shows apparent dissociation constants of 8 and 41 nM, respectively. Mean and SD of three data points for different protein concentrations are shown for $n = 3$ experiments. (B) Heparitinase treatment of perlecan shows a shift in the mobility consistent with removal of HS chains. (C) Solid-phase assay shows that binding is preserved after heparinase treatment of perlecan, even if the affinity is decreased. Mean and SD of three data points for all different protein concentrations are shown.

Reference

Miner, J.H., B.L. Patton, S.I. Lentz, D.J. Gilbert, W.D. Snider, N.A. Jenkins, N.G. Copeland, and J.R. Sanes. 1997. The laminin α chains: expression, developmental transitions, and chromosomal locations of α1-5, identification of heterotrimeric laminins 8–11, and cloning of a novel α3 isoform. *J. Cell Biol.* 137:685–701. http://dx.doi.org/10.1083/jcb.137.3.685